Arab American University - Jenin

Faculty of Graduate Studies

Lennard-Jones Molecules Using the Monte Carlo Simulations with Optimum Maximum Allowed Displacement

By

Hayel Hussein Al Shraydeh

Supervisor

Dr. Iyad Suwan

Co-advisor

Dr. Abdel-Rahman Abu-Labdeh

This thesis was submitted

in partial fulfillment of the requirements for the degree of

Master of Science

in

Applied Mathematics

February 2015

Lennard-Jones Molecules Using the Monte Carlo Simulations with Optimum Maximum Allowed Displacement

Hayel Hussein Al Shraydeh

This thesis was defended successfully on February the seventeenth, 2015 and approved by

Committee members	Signature
1. Dr. Iyad Suwan (Supervisor)	.....
2. Dr. Abdel-Rahman Abu-Labdeh (Co-advisor)	.....
3. Dr. Elias Dabeet (Internal Examiner)	.....
4. Professor Dr. Naji Qatanani (External Examiner)	.....

Dedication

I dedicate this thesis to my family and friends. A special feeling of gratitude to my lovely parents, Hussein and Hanan, my brothers Zaid, Mo'ath, Salameh, and Sahel, and my sisters Asma' and Hedayah.

Acknowledgments

First of all, I want to thank God for all his graces on me and for giving me the ability to finish this work.
It is an honor for me to work with my supervisors Dr. Iyad Suwan and Dr. Abdel-Rahman Abu-Labdeh. To them I owe my deepest gratitude.

It is my pleasure to thank those who made this thesis possible. My parents, brothers, sisters, and friends, without their support this work could not have been finished.
I would like to thank the examination committee for their valuable feedback in order to have this work brought out with the best standards.

Finally, my great gratitude to the Mathematics Department at Arab American University- Jenin.

Contents

Abstract

In this thesis, a periodic systems of N-point particles with Lennard-Jones potential are simulated by using Monte Carlo technique in three dimensional space. Since Lennard-Jones is a short range potential, it is considered to be *zero* beyond some cut off radius r^*_{cut}. The optimum r^*_{cut} found is 2.5. The maximum allowed displacement used in a Monte Carlo simulation of any N-particles system controls the convergence to the potential energy of the system at equilibrium. The optimum maximum allowed displacement is found to be associated with 50% acceptance rate; which is the ratio of accepted Monte Carlo moves to the total number of moves. An explicit mathematical formulas for the optimum maximum allowed displacement (O-d_{max}) are obtained as a function of both temperature and density. Those formulas are calculated at different values of temperature and density by fitting the Monte Carlo simulation results, using the fitting tool in Matlab.

List of Tables

List of Figures

ملخص

في هذه الأطروحة قمنا بمحاكاة نظام مكون من عدد من الجسيمات عديمة الأبعاد تحت تأثير جهد لينارد جونز في الفضاء ثلاثي الابعاد بالاعتماد على طريقة مونتي كارلو حيث قمنا بدراسة وتحليل النتائج. وحيث أن جهد لينارد جونز هو عبارة عن جهد ذو تأثير قصير المدى، الغيت قيمته على مسافة معينة يصطلح عليها بالمسافة المقطوعة. المسافة المقطوعة نظريا والمختبرة تجريبيا من ناحية الدقة من خلال هذه الدراسة هي ٢.٥ . تكمن اهمية دراسة أقصى ازاحة ممكنة للجسيم ،والمستخدمة في دراسة نظام لينارد جونز لعدد معين من الجسيمات، في التحكم في تحويل النظام الفيزيائي المدروس الى النظام المتزن. أفضل ازاحة ممكنة للجزيئ والمستخدمة فيزيائيا وجد أنها مرتبطة بمعدل قبول ٥٠ %، والذي يعرف بالنسبة بين عدد الازاحات المقبولة للجزيئات الى عدد الازاحات الكلي في طريقة مونتي كارلو. في هذه الاطروحة استنتجت معادلات رياضية لاختيار افضل ازاحة ممكنة للجزيء اعتمادا على تحليل ودراسة النتائج التي حُصل عليها من خلال اعتمادنا على طريقة مونتي كارلو تحت ظروف متعددة من الكثافة ودرجات الحرارة وباختيار أفضل النتائج المقبولة والمحددة اعتمادا على مقاييس احصائية متعددة باستخدام برنامج الماتلاب.

Chapter 1

Introduction

The Lennard-Jones (LJ) potential is one of the most important mathematical models that describes the energy of interaction between two particles, usually, neutral atoms or non polar molecules. The starting point of LJ potential comes from his insistent on Aufbau principle, which is a building up principle that gives a sequence in which various orbitals are filled up with the electrons in the increasing order of their energy [1]. In the LJ potential, however, the electron dynamics could be ignored based on Born-Oppenheimer approximation [2], which states that the electrons dynamics is sufficiently rapid, that electrons can be assumed to respond instantaneously relative to the time scale for the atomic motion [3, 4, 5, 6, 7].

The LJ potential is used to study the nature and stability of small clusters of interacting particles in crystal growth and random geometry of liquids [8, 9]. This potential also appears in molecular dynamics to simulate many particle systems ranging from solids, liquids and gases. Also, this potential appears in the study of the motion of stars and galaxies in the universe among other applications [10].

The common used form of the LJ potential between two neighboring particles is given by

$$U_{\mathrm{LJ}}(r) = 4\epsilon\left[\left(\frac{\sigma}{r}\right)^{12} - \left(\frac{\sigma}{r}\right)^{6}\right], \tag{1.1}$$

where the parameter ϵ represents the strength of the attraction between particles. The parameter σ represents the intermolecular separation at which the potential energy vanishes, and r is the distance between the two particles. This simple form of potential was originally transformed from Mies expression [11] to describe not only the atomic, but also the intermolecular interactions expressed as the sum of all possible forces between all molecules of two atoms [12].

The minimum value of the LJ potential occurs at $r_0 = 2^{\frac{1}{6}}\sigma$. If the distance between particles is greater than r_0, attraction happens between particles. However, if the distance is smaller than r_0, a repulsion happens. The first term of Equation (1.1) describes the repulsive potential between particles, and arises from Pauli's Exclusion Principle (PEP) [13]. The second term of Equation (1.1) describes the attractive potential. This part of LJ potential depends on van der Waal's forces which is the sum of the attractive forces between molecules (or between parts of the same molecule) [14].

In 1929, the subject of molecular spectra and molecular structure had attracted the attention of many scientists like, Hund F., Mulliken R. S., Raman C. V., Henri V. and Herbberg G. [15]. To this specialist audience, Lennard-Jones presented his first paper on the theory of Molecular Structure [15, 16]. He suggested that for large molecules the atoms with the inner gas structure of completed outer shells could not show bonding. Except for the London force, they must repel one another. By starting from pairs of such atoms and removing electrons one by one, Lennard-Jones could arrive the structure of these large systems.

Lennard-Jones work on intermolecular forces is best known today though his theories of liquids and of surface catalysis. Although The LJ work in molecular structure, is represented in a relatively small number of papers, but it shows better understanding of the fundamental aspects of the subject and injecting ideas which are still very useful [15].

In 1933, the molecular orbital theory had become much more accepted as a valid and useful theory. In 1934, LJ presented a paper on hydrocarbon free radicals, including CH_2, in which group theory is used to help assign the order of the orbital energies and explain the electronic and geometrical structures [15, 17].

H*ü*ckel E. [15] acknowledged that the first quantitative use of molecular orbital theory was the paper of LJ published in 1929. Perhaps this contact with H*ü*ckel prompted Lennard-Jones next molecular paper [15] on the treatment of conjugated hydrocarbons. This paper is still quoted as the formative paper in the treatment of Polyacetylene since it allowed for the continual alternation of double and single bond character despite the length of the molecule.

The first accurate calculation of a molecular orbital wave function using LJ potential was done by Coulson [15], then, his method was extended to the Lithium molecule [15]. Although Lennard-Jones gave partial explanations much earlier, the final resolution for the problem of justifying the use of atomic orbitals for the inner electrons and diatomic orbitals only for the valence electrons was not achieved until 1949. LJ showed [15] that the determinant wave function had unitary transformations which left it invariant but could be used to transform the molecular orbitals into localized equivalent orbitals without loss of accuracy. In this papers he gave a rigorous derivation of the orbital equations from the Schr*ö*dinger equation using a method he had introduced [15].

It was not until the third paper in this series [15] that molecular orbitals were

completely defined as eigenfunctions of the self-consistent field method Hamiltonian. At this point the molecular orbital theory became fully rigorous and consistent. After that, more accurate potential functions have been obtained, but LJ potential function remains widely used [18]. The LJ function is the best for modeling many systems, like inter-robot interactions, as well as interactions between robots and their environment [19].

In this thesis, N-point identical particle systems moving under the action of LJ potential are studied using Monte Carlo (MC) simulation. MC simulation is widely used to prove many theories like inverse problem theory, and it is also applied to get properties of molecular and atomic systems. It is considered as a controlled statistical sampling techniques (experiment) that is used, in conjunction with a model, to obtain approximate answers for questions about complex with multi-factor probabilistic problems.

Monte Carlo simulation has a lot of advantages, it is computationally simple scheme, and relatively modest computation times. It can also be adapted for calculations of averages in ensembles. In MC simulation, the random sampling is designated to ensure ergodicity where the ensemble average equals the time average. Thus, the system moves from a given state to any another neighboring state with equal probabilities. This sampling rests on a Markov Chain of states, whereby the outcome of the current state depends only on the previous state.

Studying systems by MC simulation occupies wide range of researchers interest. For example, Jayalatha K. *et.al*. studied Silver nano-particles with LJ potential [20]. They used LJ potential to analyze the nature of particle interaction and to estimate the cohesive energy of silver nano-particles. David M. *et.al*. studied and analyzed the LJ fluid [21]. Sesma J. solved Schrödinger equation with LJ potential by using a procedure that treats in a rigorous way the irregular singularities

at the origin and at infinity [22]. Tai-Chia Lin *et.al.* found a class of approximate Lennard-Jones (LJ) potentials with a small parameters [23]. Faro *et.al.* developed a simple pair-additive Lennard-Jones plus Coulomb potential for molecular simulations of the trivalent cation AL^{3+} in water [24]. Sergey A. *et.al.* studied liquid-solid phase transition in the Lennard-Jones system [25].

In this work, each state of the system is introduced by performing one random move of one particle of the system. The state space is defined by all outcomes. The most important parameter that determines the convergence of the Markov chain and must thus be adequately selected is the maximum displacement allowed for the particle. If the maximum displacement is too small, the phase space is explored too slowly, whereas too many states are rejected if this displacement is too large [26, 27].

The maximum allowed displacement affects the acceptance rate, which is defined by the ratio of the accepted states divided by the total number of states. Experience indicated that an acceptance rate of approximately 50% is often desirable for a MC simulation. In fact there is no theoretical basis for using an acceptance rate of 50%. In some cases it may be actually detrimental to efficient sampling. Mountain and Thirumalai proposed an algorithm for determining the efficiency of MC simulations. They reported that an acceptance ratio of 20% was twice as efficient in generating a satisfactory sample as compared with the traditional acceptance rate of 50% [28]. Wood and Jacobson also suggested that an acceptance ration of 10% maximizes the root mean square displacement of atoms as a function of computer time [29]. The main objective of this thesis, therefore, is to produce a stable computer simulations of the LJ potential by using Monte Carlo simulation, in order to get an optimum maximum allowed displacement (O-d_{max}) in three dimensional case (3D). In this work, the study of optimum maximum allowed displacement is associated with the acceptance rate of 50%.

In chapter two, LJ potential is presented in details. The important concepts, like thermodynamics, principle ensembles, statistical physics, force and potential energy, intermolecular forces and van der Waals forces, Pauli's exclusion Principle and Aufbau principle, that are essential for understanding it, are also introduced in chapter two. In chapter three, molecular simulation, statistical methods, Metropolis Monte Carlo algorithm are introduced and explained in details. Acceptance rate, maximum allowed displacement, statistical measures that are used in fitting are also discussed in this chapter. In chapter four, the simulation results are presented and discussed. The mathematical formulas for the optimum maximum allowed displacement as a function of both temperature and density, that are obtained by fitting the simulation which represents the relation between the optimum maximum allowed displacement with density and temperature are also presented in chapter four. In addition, conclusions and future plan are also discussed in this chapter.

Chapter 2

Lennard-Jones Potential

Lennard-Jones potential is one of the most important pair potentials that is used very often in many branches of science. Deep information in physics and chemistry are needed to understand this potential. This chapter presents some important concepts and definitions that are essential in understanding the origin of this potential. Therefore, the concepts of force, potential energy, intermolecular interactions, Born-Oppenheimer approximation, Paulis exclusion principle, and Aufbau principle are included in this chapter. A step by step derivation of LJ potential is also presented in this chapter. In addition, a brief discussion is done in order to show that LJ model could be universalized for any given material at any given conditions.

2.1. Thermodynamics

Thermodynamics is the science which deals with heat and its relation to other forms of energy and work. It has studied processes that manage large systems when they undergoes from one thermodynamics state to another due to change in their properties. This means that, the state of a system can be described by values of thermodynamics

parameters [30]. Thermodynamics, therefore, represents the relation between heat and motion; and it deals with the processes involving heat, work, and other forms of energy. In general, thermodynamics gives better understanding of physical systems.

Four principle laws of thermodynamics lead to the definition of the thermodynamics properties: The zeroth law, the first law, the second law, and the third law. The zeroth law of thermodynamics involves some simple definitions of equilibrium states and it implies that "if systems A and B are each in thermal equilibrium with a third system C, then A and B are also in thermal equilibrium with each other". By thermal equilibrium, we mean that the system reaches the minimum energy. The first law of thermodynamics states that "the energy can neither be created nor destroyed"; which is the statement of conservation of energy. The second law of thermodynamics states that "entropy can be created, but not destroyed". The third law of thermodynamics states that "the entropy of a pure crystalline substance is zero at the absolute zero temperature" [31, 32, 33, 34].

Our results presented in this thesis can be used to bring LJ systems to the thermal equilibrium state in an optimum way. Therefore, researchers who are working in this field, can use the present results to get low computational cost while simulating a system with LJ potential .

2.2. Principal Ensembles and Statistical Physics

In order to study various thermodynamics properties of a system from microscopic model, a new branch of physics appeared: the statistical physics (it is also called statistical mechanics). Historically, statistical physics has been developed after the thermodynamics. The main purpose of this branch of physics is computing thermodynamics properties of a system with known thermodynamics state. Statistical

mechanics also provides a theoretical framework for understanding macroscopic phenomena from the knowledge of the individual molecules composing these systems. This implies that statistical physics gives a very good understanding of macroscopic systems by studying the microscopic properties of these systems.

Statistical mechanics then used to get macroscopic system properties with fixed thermodynamics variables. Macroscopic conditions (like volume, temperature, and number of particles) are translated to microscopic world as boundary conditions or constraints. Microscopic system is defined by extensive variables (variables that scaled in size like volume or number of atoms) that are constant in macroscopic world. In this work, a microscopic system of particles is studied using mathematical and statistical methods, that will be explained in the next chapter.

A useful and important concept in statistical physics, which was introduced by Josiah Willard Gibbs is an ensemble [35]. An ensemble can be defined as a large collection of microscopic systems that share a given set of thermodynamics variables but have different molecular configurations [36]. The ensemble itself has a constant total energy E_{tot}. It has been introduced to represent a possible state that the system could be in. Each ensemble consists of one extensive and one intensive variable. In this work, canonical ensemble is used [35], where all the microscopic systems have a constant number of molecules (N), constant volume (V), and constant temperature (T). The canonical ensemble, therefore, is referred to NVT ensemble [37]. To generate a canonical ensemble, a collection of systems is placed in thermal contact with a heat path at fixed temperature. The walls of these systems allow heat transfer but not allowing molecules to pass through while maintaining a constant volume. After equilibration, the heat bath is removed and the entire collection of systems is isolated from the surroundings.

Other common ensembles, that can be used in thermal physics, are the grand

canonical ensemble (with constant chemical potential, constant volume, and constant temperature), and microcanonical ensemble (with constant number of particles, constant volume, and constant energy). For each ensemble, there is a thermodynamics state function that shares the same natural independent variables [35, 37, 38, 39]. We can keep on making other ensembles by switching in intensive or extensive variables [27, 40].

2.3. Force and Potential Energy

Physicians have defined the force as "any interaction which tends to change the motion of an object" [41], and they have defined the energy as "the ability to do work"[42]. The relation between the force and the potential energy can be illustrated as follows. When a non zero resultant force ($\vec{F}$) acts on a system, a net work (W_F) is done on this system by $\vec{F}$ [43]. Since the net work done on this system is the change in its kinetic energy (ΔE_k), then

$$\Delta E_k = W_F. \tag{2.1}$$

Forces can be classified as conservative or non conservative [44]. If a force depends only on the distance between the two particles, then this force is called conservative force. In this case, the energy produced by changing the distance between the two particles is defined as the potential energy (E_p). Because the change in the potential energy equals minus the work done by the conservative forces, Equation (2.1) can be written as [45]

$$\Delta E_k = W_{cf} + W_{ncf}, \tag{2.2}$$

Where W_{cf} and W_{ncf} denotes the work done by conservative and non-conservative forces, respectively. Equation (2.2), can also be written as

$$\Delta E_k = -\Delta E_p + W_{ncf}, \tag{2.3}$$

$$or \qquad \Delta E_k + \Delta E_p = W_{ncf}, \tag{2.4}$$

The change in the kinetic energy plus the change in the potential energy is called the change in the total energy of the system. Hence, Equation (2.4) can be written as

$$E_{total} = W_{ncf}. \tag{2.5}$$

It is worth noting that a conservative force (in general) is defined as the derivative of a potential energy with respect to position. That is [44]

$$\vec{F}_{con} = -\vec{\nabla} U(\vec{r}), \tag{2.6}$$

where $\vec{\nabla} U(\vec{r})$ is the gradient of the potential energy $U(\vec{r})$ with respect to the position $\vec{r}$.

In N-particle system, Lennard-Jones studied the energy of a particle with respect to another particles as a result of their positions [46]. In his study, he used various theories that describe the forces between the particles. The LJ potential, therefore, describes the interactions between molecules (or atoms) of a given system.

2.4. Intermolecular interactions and Van der Waals forces

Pure substances are formed of elements (elements are also grouped into metals and non-metals). All of these elements have a basic building block of atoms, which are the smallest form of an element. Atoms can also be combined to form molecules. Molecules could be founded in covalent. Covalent means a sharing of electrons between two atoms, in which their orbits overlap and they form a bond or (multiple bonds). When covalent bonding exists, molecules are produced. If the electron density is symmetric, no positive and negative poles, then the molecule is called non-polar molecule. In polar molecule, however, the electron density is antisymmetric, like hydrogen chloride (HCl). In the case of a polar molecule, one end of the molecule is positive and the other end is negative, and hence an electric dipole is induced [47]. Particles (molecules, atoms or ions) exert an attractive or repulsive forces between themselves, which is called intermolecular forces. Intermolecular forces are responsible on the existence of gases, liquids and solids in nature, and determines the physical and chemical properties of them. Intermolecular forces between neighboring particles are weak compared to the intramolecular forces, which are the chemical bonds (like covalent bond) that holds atoms together [48, 49].

The basic concepts of the quantum-mechanical theory of intermolecular forces were formulated about 90 years ago. Even though, the number of studies on intermolecular interactions are rapidly increased during the last several decades. This development has emerged for two reasons. Firstly, a general development of quantum-chemical methods of calculating the electronic structure of molecules has taken place, partly due to the availability of high-speed computers and the use of more refined

mathematical methods. Secondly, more reliable experimental methods have appeared which have allowed the theoretical predictions to be verified [50].

There are several types of intermolecular forces which due to their internal structure. Ion-Ion forces, Dipole-Dipole forces, Ion-Dipole forces, Hydrogen bonding, Induced dipole forces, and Induced Dipole-Induced Dipole forces (also called Dispersion forces). Ion-Ion forces (also called Coulomb's forces) contains electrically charged entries and it is strong as those in covalent bond. They are long ranged and it can be attractive or repulsive forces. The potential energy in this type of forces is proportional to r^{-1}, where r is the distance between the two particles. Dipole-Dipole forces resulting between polar molecules, and it can be attractive or repulsive or zero. The polar molecules are tried to align themselves such that the positive end of one molecule is near the negative end of another. It does not take a particular shape especially in gas and liquid. The potential energy between both polar molecules separated by the distance r falls off as r^{-3}. Ion-Dipole forces occurs when a polar molecule is near an ion. Positive ions are attracted by the negative end of the dipole and repelled by the positive end. Hydrogen bonding forces are the strongest intermolecular forces which occurs when a hydrogen atom bonded to a smallest highly electronegative atom, such as Oxygen, Nitrogen, or Fluorine. Induced Dipole forces occurs between non polar molecules and atoms where the electrons are symmetrically distributed. The electron distribution can be distorted by approaching electrical charge as follows. If we have an atom that has electrons with symmetrically distribution and another positive charged ion approaching to that atom, the ion will attracts the electrons on the side near it more strongly than the electrons on the far side, and that will induced a temporary dipole moment in the atom. The Induced Dipole forces are weak and are effective only at short range. Dispersion forces are occurs between neutral atoms or non-polar molecules, and they are always attractive. Such a temporary dipole on one molecule

will induce a temporary dipole in the other molecule. Dispersion forces are falls off as r^{-6}, so that they are short ranged [49, 51, 52, 53].

In general, attractive intermolecular forces that are between the same substance is called cohesive force. Force of cohesion is maximum between solid molecules, less between liquid molecules and least between gas molecules (zero in ideal gas). Because of this reason, solids and liquids have definite volume while gases have no fixed volume. The force of attraction between different substance is called adhesive force. Because of this force, the water sticks to the glass and gum sticks to the paper [54].

On the other hand, the repulsive intermolecular forces arise between particles is due to the electron clouds when they start overlapping. The repulsive forces increases much more sharply with decreasing separation in comparison to the attractive intermolecular forces. However, the repulsive forces range is much shorter than that of the attractive one [55]. Two mathematical models are used to describe repulsive forces. The exponential form, $Ae^{-r/\rho}$, which is successful in applications when A and ρ are chosen to fit experimental data. The second mathematical form is the inverse power r^{-n}, where n is quite large, is also successful in many applications[52].

Van der Waals forces is a term used to describe some types of attractive intermolecular forces that acts between particles (molecules or atoms). Van der Waals have two main characteristics: they are weak and additive. Several explanations for Van der Waals have been proposed. In 1920, Debye presented Debye force, (also called induction force) to describe the attractive Dipole-Induced Dipole force. In 1921, Keesom presented Keesom force (also called dipole orientation force) to describe the attractive Dipole-Dipole forces . In 1930, London presented what is called London force (or dispersion force) to describe the attractive Dispersion force [56].

Lennard-Jones has considered the Van der Waals forces in deriving the attractive part of his potential. Therefore, the LJ potential consists of two parts, attractive

and repulsive. The attractive part has been derived based on Van der Waals forces between non-polar molecules as will as between neutral atoms [49, 57]. While for the repulsive part, the choice of $n = 12$ in inverse power form r^{-n} is widely used [52].

Since LJ potential could be applied to particles, the issue arises is the applicability of LJ potential on electrons. The well known Born-Oppenheimer(B-O) approximation [58], which is the most important method for determining molecular wave functions and associated energies allows to model the system by LJ potential with ignoring the electrons movements. In general, B-O approximation assumes that the low-mass, (rapidly moving, negatively charged electrons) can immediately adjust their distribution to the positive potential of slowly moving (heavy, massive nuclei).

2.5. Pauli's Exclusion Principle

In the empirical study of atomic spectra, Pauli has discovered a simple generalization which is applicable to all atomic spectra in 1925 [59]. He noticed that there are four quantum numbers assigned to each electron. The first quantum number is commonly known as the principal quantum number. This number is integer and was used in establishing Bohr's model. The second number is called, the azimuthal angular momentum. It refers to the sub-shells or (sub-levels) that occur within each principal energy level in the atomic spectrum. The third number is the magnetic one. The magnetic quantum number specifies the particular orbital within a sub-shell where an electron is highly likely to be found at a given point in time. The forth number is called the spin quantum number. The spin of the particle is its essential angular momentum and a characteristic of a particle.

Pauli's Exclusion Principle states that "no two electrons in any atom can share the same set of four quantum numbers", where the quantum numbers describe the

possible states that the electrons can occupy in an atom [60, 61]. This was a paradoxical discovery at the time it was made, because it preceded the hypothesis of electron spin, which leads to the interpretation of the fourth quantum number. Although interpretation of this quantum number in terms of electron spin was soon given, the meddlesome fact remains that the two individual sets of four quantum numbers of each of two electrons cannot be alike. This is known as Pauli's Exclusion Principle (PEP) [13, 62]. The PEP states that as quantum states filled up, electrons are kept further and further from the nucleus. This is balanced by the attractive electric force between the electron and positively charged nucleus. Therefore, two electrons cannot occupy the same quantum state. This means that, two identical electrons cannot occupy the place at the same time with the same orientation.

The PEP has been derived only in relativistic quantum mechanics using the spin statistic theorem. Although the PEP is physically correct, but the reason of this correctness is still unknown. Some hypotheses say that the PEP repulsive comes from an extremely strong virtual particle exchange on very short distance scales [63]. Some theorists say that it is caused by an anti-symmetric wave function [63]. Examples of particles that obey PEP are electrons and neutrons, while bosons and protons do not obey this principle.

PEP was the origin of Aufbau principle. Aufbau is a German word which means building up or construction. This is the reason that this principle is also known as building up principle (or the construction principle). This principle gives us the manner in which various orbitals are filled up with the electrons in an increasing order of their energies [64]. Lennard-Jones has considered the Pauli Exclusion Principle (PEP) to state the repulsive part of his potential.

2.6. Lennard-Jones Potential

The energy models are divided into three categories, empirical models (which are functional forms with parameters fitted to experimental or calculated data), the semi-empirical models (which are quantum mechanical in form but empirical in parameters), and the quantum mechanical models (which start from Schrödinger equation and then make approximation of the solution). The LJ potential model is an empirical one. In empirical models, in some scene, the only need is to take some form for the energy and fit it to any data. Sometimes, the data is quantum mechanically computed.

The LJ potential has been proposed based on the material physics. It is used to model interactions of a punch of particles (molecules or atoms) and sum there energy from pairwise interactions which depend on the distance between any two particles. The LJ potential is attractive at relatively long distances and repulsive at short distances.

In this work, LJ potential with the two-particle interactions are considered in calculations. That is, the pairwise force between two particles is unaffected by the positions of the other particles. This kind of approximation is suitable for gases, and liquids. In this work, the intermolecular forces are also assumed to be independent of the molecules (or atoms) velocities.

In general, the intermolecular potential energy U_{tot} is the sum of two-particle contributions and is given by

$$U_{tot} = \sum_{i=1}^{N-1} \sum_{j=i+1}^{N} U(r_{ij}), \tag{2.7}$$

where the function $U(r_{\mathrm{ij}})$ is the pair potential energy function of particles i and j,

r_{ij} is the distance between the centers of particles i and j, and N is the number of particles in the system. The simplest pair potential energy form $U(r_{ij})$ between particles i and j, that is commonly used is the LJ potential, is given by

$$U(r_{ij}) = 4\epsilon\left[\left(\frac{\sigma}{r_{ij}}\right)^{12} - \left(\frac{\sigma}{r_{ij}}\right)^{6}\right], \tag{2.8}$$

where the parameter ϵ represents the strength of the attraction between particles. The parameter σ represents the intermolecular separation at which the potential energy vanishes [65].

The first term of Equation (2.8) is repulsive. This happens when the particles become close together, where the electron clouds overlap. In this case, the electrons can not occupy exactly the same quantum state according to PEP [66, 67, 68], as mentioned before. The second term of Equation (2.8) is attractive and comes from the interaction between fluctuating dipoles, like atoms with filled electron shills (as noble gases).

In fact, there is no physical justifications for r^{-12} that Lennard-Jones has used for repulsive part. The power 12 makes it easy to calculate the potential since it is the square of r^6 which is already calculated [69, 70, 71, 72]. In the following argument the second term of LJ potential is derived . The LJ potential is a form of Mie potential, which has the form [11]

$$U(r) = \frac{A}{r^m} - \frac{B}{r^n}. \tag{2.9}$$

In Bohr atom, an electron is pictured as orbiting around a proton. The smallest distance between the electron and proton is known as the first Bohr radius a_o and is the radius at which the Coulomb energy $\frac{e^2}{4\pi\varepsilon_o a_o}$ is equal to $2hv$. That is

$$a_{\mathrm{o}} = \frac{e^2}{4\pi\varepsilon_o 2hv}, \tag{2.10}$$

where v is the electronic absorption frequency, $v = 3.3 * 10^{15} s^{-1}$, so that $hv = 2.2 * 10^{-18} J$. This is the energy of an electron in the first Bohr radius and is equal to the energy needed to ionize the atom. The Bohr atom has no permanent dipole moment, however, at any instant there exists an instantaneous dipole of moment, given by

$$U = a_{\mathrm{o}} e. \tag{2.11}$$

Whose field will polarize a nearby neutral atom, giving rise an attractive interaction that is entirely analogous to the dipole-induced dipole (Debye) interaction. The energy of this interaction in a vacuum will therefore be given by [73, 74]

$$U_{Debye} = \frac{-u^2 b_o}{(4\pi\varepsilon_o\varepsilon)^2 r^6}, \tag{2.12}$$

where b_{o} is the electrostatic polarizability of the second Bohr atom, ε is dielectric permittivity, which is given by [75]

$$b_{\mathrm{o}} = 4\pi\varepsilon_{\mathrm{o}} R^3, \tag{2.13}$$

where R being the radius of the atom which is (in this case) the Bohr radius a_{o}. Equation (2.13) is approximately $4\pi\varepsilon_{\mathrm{o}} a_{\mathrm{o}}^3$. Using this expression for b_{o} and Equation (2.10) for a_{o}, the preceding interaction energy can be written as

$$U(r) = \frac{-b_{\mathrm{o}}^2 hv}{(4\pi\varepsilon_{\mathrm{o}})^2 r^6}. \tag{2.14}$$

Except for a numerical factor, Equation (2.14) is the same as that derived by London in 1930 using quantum mechanical perturbation theory. London's famous expression

for the dispersion interaction energy between two identical molecules (or atoms) is

$$U(r) = -\frac{3}{4}\frac{b_o^2 h v}{(4\pi\varepsilon_o)^2 r^6}. \tag{2.15}$$

The stabilizing repulsive of LJ potential has no real scientific justification; it is basically just a repulsive potential to make sure that the particle is repulsive at close distances. It is related to Pauli's Exclusion interactions which are (usually) follow an exponential function

$$U(r) = e^{(-\frac{r_o}{r})}. \tag{2.16}$$

But for simplicity, they are usually modeled as power laws

$$U(r) = -\frac{r_o}{r^n}, \tag{2.17}$$

where n is in between 9 and 12. Although the commonly used power in Equation (2.9) are $n = 6$ and $m = 12$, the researchers in this field can use different values of those powers [72], for example $n = 3$ and $m = 9$. But those choices may problematic, since those powers depends sometimes on the structure of the material.

To get the minimum of LJ potential, $\frac{\partial U}{\partial r}$ must be zero. This happens when r= $r_{\min}$. So, $r_{\min}$ must satisfy the condition

$$2\left(\frac{\sigma}{r_{\min}}\right)^{12} = \left(\frac{\sigma}{r_{\min}}\right)^{6}. \tag{2.18}$$

That is

$$r_{\min} = 2^{\frac{1}{6}}\sigma. \tag{2.19}$$

Therefore, the minimum potential energy $U(r_{\min})$ is given by

$$U(r_{\min}) = -\epsilon. \tag{2.20}$$

When expressing temperature, pressure and density in normalized units, as shown in Table (1.1) [27], all LJ systems are identical. The LJ model for a given material in reduced unites always equals to the LJ model for another material at different conditions of temperature and pressure.

Table 2.1: Reduced unites that can be used generally in any LJ model for a given material

Property	*Real*	*Reduced*
Length	$\frac{r}{\sigma}$	r^*
Density	$\frac{N}{V*} = \frac{N\sigma^3}{V}$	ρ^*
Temperature	$\frac{TK_B}{\epsilon}$	T^*
Energy	$\frac{U}{\epsilon}$	U^*
Pressure	$\frac{P\sigma^3}{\epsilon}$	P^*

In terms of reduced units, Equation (2.8) becomes

$$U^*(r^*) = 4\left[\left(\frac{1}{r^*}\right)^{12} - \left(\frac{1}{r^*}\right)^{6}\right], \tag{2.21}$$

where $r^* \in R^n$.

Figure (1) represents the LJ potential between two particles in reduced unites. As seen in Figure (1), the minimum occurs at $r^*_{\min} = 2^{\frac{1}{6}}$, and at that distance the reduced minimum potential energy equals to -1.

One of the good advantages of a LJ potential is that it falls off quickly, and only those particles within a nearby environment have much effect. As a result, it is possible to limit (or cut off), the maximum range of the interaction. The choice of the reduced cut off distance r^*_{cut} of LJ potential energy, which is commonly used, is

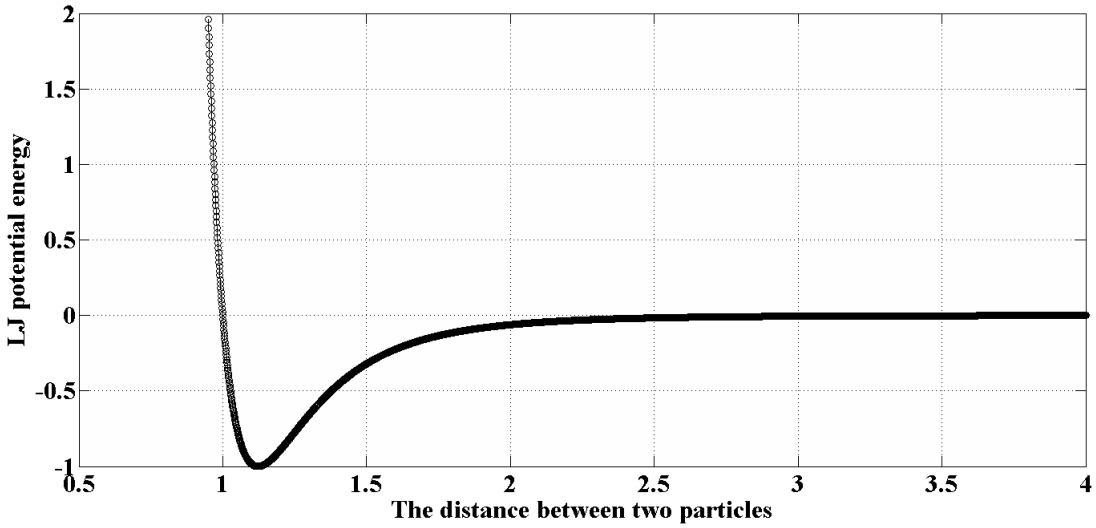

Figure 1: LJ potential energy between two particles in reduced unites. The reduced distance (r^*) is ranging from 0.95 to 3 with step size 0.01

in the range 2 and 3 [76, 77]. A typical value for this distance is $r^*_{cut} = 2.5$ [78].

The LJ potential potential shown by Equation (2.21) is used in its truncated and shifted form for all simulations. This method requires applying an energy correction during the calculation of the potential energy. This energy correction is [27]

$$U^*(r^*) = \left\{ \begin{array}{cc} 4\left[\left(\frac{1}{r^*}\right)^{12} - \left(\frac{1}{r^*}\right)^{6} \right], & \text{if } r^* \leq r^*_{cut} \\ 0, & \text{if } r^* > r^*_{cut} \end{array} \right\}. \tag{2.22}$$

Chapter 3

Monte Carlo Simulation

3.1. Introduction

Recently, the method of modeling and computer simulation has become a bridge between the theoretical and experimental branches of science. Modeling and computer simulation are important in understanding the behavior of the parts of a system, and of the system as a whole [79]. Mathematical models are theoretical structures that describe the behavior of real systems through the quantification and manipulation of variables [80], where simulation is essentially a controlled statistical sampling technique that is used, in conjunction with a model, to obtain approximate answers for questions about complex probabilistic problems [81].

The importance of the modeling and computer simulation comes from different reasons. One of the most important reasons, is controlling parameters, which gives a quick understanding of the behavior of the system. Modeling and computer simulation, give the possibility to predict results before testing the system in real life. Modeling and computer simulation are used when the experiment is too hard to be done either physically or financially. By modeling and computer simulation, we

can systematically investigate, prove or disprove hypothesis. Thus, they complement both theoretical and experimental research [82].

Monte Carlo is considered to be the most important simulation technique, that is usually used for solving problems in statistical physics. In Monte Carlo technique, the basic idea is to evaluate thermal averages of materials by statistically sampling desired region of the phase space of a model using computers. Therefore, the use of probability and statistics is essential in statistical physics [83].

The quick development of computational resources, and the expansion of new algorithms, allow Monte Carlo simulations to be a base for studying lots of subjects of statistical physics [84]. One of the most challenges and difficulties that face the computer simulations is the computer speed and computer memory [76].

The results of this work are based on Monte Carlo simulations. Hence, a brief look at the general idea behind equilibrium thermal Monte Carlo techniques is done in this chapter. Four important ideas are introduced: importance sampling, transition probability, detailed balance, and the Metropolis algorithm. In addition, this chapter presents goodness of fit and difficulties in computer simulations.

3.2. Molecular Simulation and Statistical Methods

Molecular simulation, is a term including both Monte Carlo (MC) and Molecular dynamics (MD) computing methods. Molecular simulation is primary used to provide exact results for statistical mechanical problems in preference to approximate solutions. The feature that distinguishes molecular simulation, from other computing methods and approximations is that, the molecular simulation of the system, is done in accordance with a very strict and demanding calculation of intermolecular energies or forces. Molecular Simulation can be described as a Computational Statistical

mechanics. It allows to determine macroscopic properties by evaluating exactly a theoretical model of molecular behavior using a computer programs.

The main difference between both implementations (MC and MD) is that in MD, the Newtonian equations of motion has to be integrated in some scheme. Contrarily in MC, a scheme to accept or reject configurations of the system, which have been generated through random processes, is needed [85, 86].

Different ways used in MD and MC simulations for calculating certain chemical or physical properties. In MD simulation, one way is tracking a certain property over time, so we can calculate a certain property for a given microscopic state for a given configuration. The microscopic averages for a certain property, and their integral over time then, can be calculated over time.In that average, only states that can be reached with the MD simulation are included, since we simulate over a finite time. This means that, averages only include phenomena that occurs in the time scale of MD simulation. If we want averaged properties over long time; statistical sampling may be more efficient. In this case, it may be better to use statistical methods such as Monte Carlo techniques.

In Monte Carlo simulations, the idea is to sampling microscopic states, that is statistically significant for long- time averages. In order to perform a sample in any statistical method, two things we have to be decided: which population we sample from, and with what probability we sample them [27, 87].

In this thesis, the MC program has main routine which is containing the main MC procedure and it contains subroutines which are called during the running of the program. Data analysis is performed by saving the results of the simulations to excel files and analyze them in Matlab.

Considering problems of statistical mechanics, we may be attempting to sample a region of phase space in order to estimate certain properties of the model. The

task of equilibrium statistical mechanics is to calculate thermal averages of interacting many-particle systems. MC simulations can do that, taking proper account of statistical fluctuations and their effects in such systems. Unlike in the application of many analytic techniques, the improvement of the accuracy of Monte Carlo results is possible not just in principle but also in practice. Therefore, the range of different physical phenomena which can be explored using Monte Carlo methods is exceedingly broad [28, 27, 76, 88, 89].

3.3. Metropolis Monte Carlo Algorithm

Modern form of MC simulation originated with Ulam and Segré in Los Alamos and ENIAC computer (but really goes back to Fermi) [90]. Before that, sampling was used as a method for integration of functions, Comte de Buffon (1777) [91].

Many ways of sampling are exists. The most important ways of sampling is simple sampling and importance sampling. In simple sampling, M states are randomly picked up from ensemble, and average property is then calculated. The basic idea of importance sampling is to sample the important states, in MC simulation. The state with low energy and fluctuates around it will founded, and the states will be picked up with a biased probability [27].

The main purpose of equilibrium statistical mechanics is calculating observable quantities of the material. This needs to average an observable quantity Q, as in the canonical ensemble, over all of the states of the system, and weighting each by the Boltzmann probability [92, 93]:

$$P(n_i) \propto e^{(-E_{n_i}/T)}, \tag{3.1}$$

where E_{n_i} is the energy of the system in state n_i, T is the temperature measured in

unites of $1/k_B$, and k_B is the Boltzmann constant. Therefore, the average value of Q is given by:

$$\langle Q \rangle = \frac{\sum_{n_i} Q_{n_i} e^{(-E_{\mathrm{n}_i}/T)}}{\sum_{n_i} e^{(-E_{\mathrm{n}_i}/T)}}, \tag{3.2}$$

such that Q_{n_i} is the value of Q at some state n_i.

Except for a few systems, the exact solution of such quantities is impossible. To obtain a good estimates of important thermodynamical variables, approximations are required. One way is to evaluate the quantity given in Equation (3.2) by summing over a large but finite number of states. With the advent of modern computers, this approach becomes more practical. The question is, how to choose a finite number of states in order to obtain an accurate estimate of Q, The simplest choice is to pick all of these states at random with equal probability from the phase space of the system. Although the simplicity of this choice, averaging over them is not likely to get any reasonable estimate of the average value of Q, since most of these randomly chosen states will not make a statistically considerable contribution to the sums given by Equation (3.2).

This means that a few terms of the sums given by Equation (3.2) will be controlling. For example, at low temperatures, the system spends almost all of its time in the ground state, or at one of the lowest excited states, as there is not enough thermal excitation to excite the system passes through every state during the measurement, even though every state appears in the sums of Equation (3.2). It cannot be supposed that the system passes through every state during the simulation. However, if instead of choosing the states at random with equal probability, they are selected based on some probability distribution $P(n)$, then it is possible to improve the accuracy of the estimate provided by averaging over these states.

The importance of this approach lies in the ability to choose the probability

$P(n_i)$ such that the selected states used in the evaluation of $\langle Q \rangle$ are statistically considerable. This approach is called as importance sampling. Suppose we choose a subset $\{n_1, n_2, ..., n_M\}$ at random, each with probability $\{P(n_1), P(n_2), ..., P(n_M)\}$, then the best estimate of Q will be given by [93]

$$\langle Q \rangle_M = \frac{\sum_{n_{i=1}}^{M} Q_{n_i} P_{n_i}^{-1} e^{(-E_{n_i}/T)}}{\sum_{n_{i=1}}^{M} P_{n_i}^{-1} e^{(-E_{n_i}/T)}}, \tag{3.3}$$

as a result, Equation (3.3) shows that the estimation of $\langle Q \rangle$, which is $\langle Q \rangle_M$, becomes more accurate as the number of the selected states M increases. In addition, when M goes to infinity, $\langle Q \rangle_M$ goes to $\langle Q \rangle$. Boltzmann distribution given by Equation (3.1), would be the most simple and efficient choice of P_{n_i} in Equation (3.3), which is a probability distribution with many applications in physics and chemistry. It forms the basis of the kinetic theory of gases, which explains many fundamentals gas properties [94].

$\langle Q \rangle_M$ then becomes just a simple arithmetic average:

$$\langle Q \rangle_M = \frac{\sum_{n_{i=1}}^{M} Q_{n_i}}{M}, \tag{3.4}$$

The choice of the Boltzmann distribution assure that the average of Q is calculated using the most statistically significant states. Markov process is the best procedure to use to select states according to the Boltzmann probability. It can be described as a series of random states such that the current state n_{i+1}, depends on the previous state n_i [95]. Markov process is a stochastic process, where future states are independent of the past states and depends only on the present state. It could be be recurrent, where if starting from n_i, there is a way of returning to the same state. If it is not recurrent, then its called transient [96, 97]. In this process, successive states n_{i+1} are generated from the previous states n_i through a transition probability, $W(n_i \rightarrow n_{i+1})$,

such that in the limit, $M \to \infty$, the distribution function of the states generated by this Markov is given by the Boltzmann distribution. Such a process have to satisfy the following four conditions [27]:

1. The state n_{i+1} is generated every time is determined by the state n_i.

2. The transition probabilities must satisfy the constraint

$$\sum_i W(n_i \to n_{i+1}) = 1 \tag{3.5}$$

3. Reaching any state of the system from any other state is possible if the program is run for a long enough time(i.e., the condition of ergodicity).

4. In equilibrium, the rate at which the system makes transitions into and out of any state n_i must be equal(i.e., the condition of detailed balance).
   Mathematically, the condition of detailed balance can be written as

$$P(n_i)W(n_i \to n_{i+1}) = P(n_{i+1})W(n_{i+1} \to n_i) \tag{3.6}$$

Using the Boltzmann probability distribution given by Equation (3.1), Equation (3.6) thus gives

$$\frac{W(n_i \to n_{i+1})}{W(n_{i+1} \to n_i)} = \frac{P(n_{i+1})}{P(n_i)} = e^{(-(E_{n_{i+1}} - E_{n_i})/T)} \tag{3.7}$$

Equation (3.7) indicates that the transition probability ratio for a move from state n_i to n_{i+1} depends only on the energy difference, $E_{n_{i+1}} - E_{n_i}$. One simple and efficient choice for the transition probability which satisfies Equation (3.7) is the Metropolis algorithm [98]. This algorithm was proposed by Metropolis and his co-workers in 1953 in the simulation of hard-sphere gases [98]. In this optimal algorithm the transition

probability from the state n_i to n_{i+1} is given by

$$W(n_i \to n_{i+1}) = \begin{cases} e^{(-(E_{n_{i+1}} - E_{n_i})/T)}, & \text{if } E_{n_{i+1}} > E_{n_i} \\ 1, & \text{if } E_{n_{i+1}} \leq E_{n_i} \end{cases} \tag{3.8}$$

In fact, a sequence of states is build up, then a property will be sampled over these states. That property will be a function of sampling.

In this work, LJ potential energy has considered as a function of MC sweeps. Typically, the first part was cutoff and removed, as the simulation started at random state, the energy was faraway from the law energy state, and so, by cutting that off, much faster relaxation of the average has been gotten, as in the first states the energy was very high. Thus, after the system being in the equilibrium, the averages has been calculated.

One aim of MC simulations is to detect phase transition at which we can get physical properties. In MC simulations, we have enormous degrees of freedom about the moves we do, these are essentially the perturbations we attempt to get to the next state in the Markov chain.

In Metropolis algorithm, a new state n_{i+1} will be selected, which has an energy lower than or equal to the present state n_i, the transition to that state is accepted. If the new state has a higher energy, it may be accepted with the probability given in Equation (3.8). To accept or reject a new state which has a higher energy than the previous one, a uniform random number $\xi \in [0, 1]$ is chosen. If the transition probability is greater than ξ, then the new state is accepted and the system moves to the n_{i+1} state. Otherwise, the new state is rejected and the system stays in the n_i state.

In fact, the choice of moving from states n_i to n_{i+1} has much freedom, which are limited by the condition that W is symmetric ($i.e, W(n_i \to n_{i+1}) = W(n_{i+1} \to n_i)$).

If many degrees of freedom is changed simultaneously, the transition probability will has so small value, and thus, the system may largely remain in its previous state as most of the desired moves would not be selected at all. Hence, one efficient and simple strategy is to change only one degree of freedom, such as moving only one particle at a time in LJ system.

Therefore, the optimal Metropolis algorithm used in the present work proceeds according to the following eight steps:

1. Choose the initial state, n_i, of the system.

2. Generate a new state, n_{i+1}, by changing one particle position randomly.

3. Compute the difference in the energy, ΔE, between the new state and the old one ($i.e, \Delta E = E_{n_{i+1}} - E_{n_i}$).

4. Calculate the transition probability according to Equation (3.8).

5. Generate a uniform distribution random number, ξ, between zero and one.

6. Compare ξ with calculated $W(n_i \rightarrow n_{i+1})$. If $W(n_i \rightarrow n_{i+1})$ is greater than ξ accept the move, otherwise leave the particle position as it is and retain the old configuration.

7. Repeat steps 2-7 as necessary.

8. Store the required observable quantities of the system every n^M Monte Carlo sweep per particles number (MCS/N) to calculate the averages.

For more details about MC procedure, excellent texts on this subject could be reviewed [82, 83, 99].

Since simulations are applied to infinite systems, boundaries of the lattice could be treated. Because the short-range interactions in the simulations have been considered, problems of finite size may be treated easily by applying periodic boundary conditions. The calculations in this thesis based on the potential energy between the particles, the total energy that mentioned earlier in this chapter is considered to be the total potential energy U_{tot} [27, 83, 87, 93, 100, 101].

3.4. Acceptance Rate and Maximum Allowed Displacement

The most important parameter in Metropolis algorithm, which has to be chosen carefully is the particles displacement vector. Given the present state n_i, a particle is picked up and randomly moved to get the new state n_{i+1}. The energy of each state has been calculated, and then the Metropolis algorithm acceptance criteria is used to get the accepted state.

The particles displacement vector affects important properties of the Monte Carlo simulation, and it is needed to adjust optimally, as it affects the efficiency of the particles moves. In fact, By choosing optimum maximum allowed displacement d_{max}, the most efficient sampling procedure will be achieved, and the Monte Carlo simulation converges in the optimum behavior, thus the fast equilibration times will be satisfied, and fast relaxation times and correlation times will be obtained, as shorter runs required to produce averages of good statistical quality.

The optimum allowed displacement move leads to high statistical accuracy, and saving lot of time needed to obtain the desired averages in an optimum simulation convergence, without affecting the equilibrium values [92].

Two main conditions the displacement vector has to satisfy. It must be chosen

randomly, and that can be achieved by random number generator in the computer. Also, its magnitude has to be chosen carefully, where the magnitude of moving is defined by $\delta = d_{max} \cdot (\vec{1} - 2 \cdot \vec{\xi})$, may be out of the whole box length, or it may be very small length, this depends on d_{max}.

The displacement move of a particle in every Metropolis MC sweep is defined by [98]:

$$\vec{r}_i^{new} = \vec{r}_i^{old} + d_{max} \cdot (\vec{1} - 2 \cdot \vec{\xi}), \tag{3.9}$$

where $\vec{r}_i^{new}$ and $\vec{r}_i^{old}$ are the new and old locations of particle i respectively. d_{max} is the maximum allowed displacement, $\vec{\xi} \in [0,1] \times [0,1] \times [0,1]$. The probability of this move using Equation (3.8) will be given by

$$W(\vec{r}_i^{old} \rightarrow \vec{r}_i^{new}) = min\left[\mathbf{1}, \frac{P(\vec{r}_i^{new}|\mathbf{R}_i)}{P(\vec{r}_{\mathrm{i}}^{old}|\mathbf{R}_i)}\right]. \tag{3.10}$$

Here, $P(\vec{r}_i|\mathbf{R}_i)$ is the conditional probability to find the particle at the position $\vec{r}_{\mathrm{i}}$ when locations of all other $N-1$ particles, defined by the set $\mathbf{R}_i = \{\vec{r}_1, ..., \vec{r}_{i-1}, \vec{r}_{i+1}, \vec{r}_N\}$, are fixed:

$$P(\vec{r}_i|\mathbf{R}_i) = const \cdot e^{\left[-\frac{1}{K_B} \sum\limits_{j=1, j\neq i}^{N} U(\vec{r}_i - \vec{r}_j)\right]}, \tag{3.11}$$

where $U(\vec{r}_i - \vec{r}_j)$ is the energy of a two-body interaction. As shown from Equation (3.9) and Equation (3.10). The acceptance ratio, which is defined as a ratio of the number of accepted states to the total number of states in a given Monte Carlo run, depends on the maximum allowed displacement d_{max}. If the magnitude of d_{max} chosen to be big, a lot of particles movements will not going to be accepted. On the other hand, if it is chosen to be small, neighbors configurations will be highly correlated, since all the states in the Markov chain are the same, and any essential change of the configuration will need many particles displacements [98]. Both cases

lead to increasing the computational work.

The optimum acceptance rate that commonly used in simulation without theoretical basis, is between 0.3 and 0.5 [27, 76, 89]. Three different definitions follow to define the optimum acceptance rate (or maximum allowed displacement).

1. The first definition was proposed in [102]. It was suggested that the optimum value of d_{max} corresponds to the maximized diffusion. The mean square particle displacement at Monte Carlo cycle m is defined as

$$< r_m^2 >=< |\vec{r}_i(m) - \vec{r}_i(0)|^2 >, \tag{3.12}$$

where $\vec{r}_i(0)$ is the initial position of the particle i and $\vec{r}_i(m)$ is the particle position after cycle m, and the averaging is taken over all particles. The self diffusion coefficient, defined by

$$D_{self} = const \lim_{m\to\infty} \frac{< r_m^2 >}{m}, \tag{3.13}$$

is used to measure the diffusion, and the value of the acceptance ratio corresponding to maximum D_{self} is considered as optimum. Based on Equation (3.13), the conclusion of [103, 104, 105] is that the optimal value of the acceptance ratio is between 0.3 and 0.4.

2. Another measure was proposed in [106], and is rested on the measurement of normalized autocorrelation function for an observable $A(m)$:

$$\psi_A(m) = \frac{< A(m) - A(0) > - < A >}{< A^2 > - < A >^2}, \tag{3.14}$$

Actually, the function $\psi_A(m)$ is used to determine the strength of a correlation

between two values of a quantity sampled at two different times. The common approximation for the autocorrelation function is given by [107]

$$\psi_A(\tau) \approx e^{-\frac{\tau}{\tau_{A,dcor}}}, \tag{3.15}$$

where $\tau_{A,dcor}$ is the de-correlation time. It is easy to see that in this approximation

$$\tau_{A,dcor} = \int_0^\infty \psi_A(\tau) d\tau. \tag{3.16}$$

Therefore, the decorrelation time can be estimated by:

$$\tau_{A,dcor} = \frac{1}{2} + \sum_2^\infty \psi_A(i). \tag{3.17}$$

The optimal acceptance rate in this approach corresponds to minimum de-correlation time. It was shown in [106], using common Monte Carlo method, that the acceptance rate of 0.5 yields minimal de-correlation time.

3. Another measurement that can be used for the optimal acceptance rate is the relaxation time, which is the time beyond which, on the average, serial correlations are disrupted. For an observable A, the relaxation is described by the function [107]

$$R_A(m) = \frac{A(m) - A(\infty)}{A(0) - A(\infty)}. \tag{3.18}$$

In order to reduce statistical errors in the calculation of the relaxation function $R_A(m)$, it is reasonable to perform some number of Monte Carlo runs starting from the same initial configuration but with different sequences of random numbers. The relaxation function averaged over these runs $R_A(m)^{av}$ can be used to

estimate the relaxation time similar to 3.17:

$$\tau_{A,rel} = \frac{1}{2} + \sum_{2}^{\infty} R_A^{av}(i). \tag{3.19}$$

3.5. Goodness of fit

Most regression software packages used in the present work, $Toolbox^{TM}$ in Matlab, generate so-called goodness of fit measures. These measures describe how well a statistical model fits a set data. Below some of these measures:

- The sum of squares due to error (SSE), which is explained as follows, for the i^{th} observation, the difference between the observed value of the dependent variable, y_{i}, and the predicted value of the dependent variable, $\hat{y}_{\mathrm{i}}$, is called the i^{th} residual. The i^{th} residual represents the error in using, $\hat{y}_{\mathrm{i}}$, to predict y_{i}. Thus, for the i^{th} observation, the residual is y_{i} - $\hat{y}_{\mathrm{i}}$. The sum of squares of these residuals or errors is the quantity that is minimized by the least squares method. This quantity, also known as the sum of squares due to error, is denoted by SSE [108]

$$SSE = \sum (y_{\mathrm{i}} - \hat{y}_{\mathrm{i}})^2 \tag{3.20}$$

- R-square (R^2), which is the percentage of the total variation in the dependent variable that is explained by the regression model. A higher R^2 means that the model explains more of the variation in the dependent variable. In the extreme, if the model were a perfect fit, the R^2 would attain its maximum possible value of 1. If the model explained none of the variation in the dependent variable,

the R^2 would attain its minimum possible value of 0 [110].

$$R^2 = \frac{SSR}{SST}, \tag{3.21}$$

where (SSR) is the sum of squares due to regression, and (SST) is the total Sum of Squares.

To measure how much the y_{i} values on the estimated regression line deviate from $\tilde{y}_{\mathrm{i}}$, another sum of squares is computed. This sum of squares, called the sum of squares due to regression, is denoted by SSR [108]

$$SSR = \sum (y_{\mathrm{i}} - \tilde{y}_{\mathrm{i}})^2. \tag{3.22}$$

The Total Sum of Squares (SST) is the difference between the observed data and the mean value across all observations [109].

$$SST = SSR + SSE \tag{3.23}$$

- Adjusted R-square, which is developed as it is shown mathematically that R^2, the coefficient of determination, can only increase when add predictors to the regression model. No matter how irrelevant it is for the response y, any new predictor can only increase the proportion of explained variation. Therefore, R^2 is not a fair criterion when compared models with different numbers of predictors (k). Including irrelevant predictors should be penalized whereas R^2 a fair measure of goodness-of-fit is the adjusted R-square which is a criterion of variable selection.It rewards for adding predictor only if it considerably reduces

the error sum of squares

$$\text{Adjusted R-square} = 1 - \frac{SSE/(n-k-1)}{SST/(n-1)}. \tag{3.24}$$

Comparing with R^2, adjusted R-square includes degrees of freedom into this formula. As a result, R^2 always increases when a new variable is added whereas R^2_{adj} may decreases. The adjusted R-square statistic can take on any value less than or equal to 1, with a value closer to 1 indicating a better fit. Negative values can occur when the model contains terms that do not help to predict the response [111].

- Root mean squared error (RMSE), which is the square root of mean squared error (MSE). RMSE measure the differences between values predicted by a hypothetical model and the observed values. In other words, it measures the quality of the fit between the actual data and the predicted model. RMSE is one of the most frequently used measures of the goodness of fit of generalized regression models. In the application of regression models, unless the relationship or correlation is perfect, the predicted values are more or less different from the actual observations. These differences are prediction errors or residuals. These residuals are measured by the vertical distances between the actual values and the regression line. Large distances are indicative of large errors. To acquire RMSE, one can square and average the individual prediction errors over the whole sample. The average of all the squared errors is the MSE. As the square root of a variance (MSE), RMSE can be interpreted as the standard deviation of the unexplained variance.

$$RMSE = \sqrt{MSE} \tag{3.25}$$

Thus, RMSE is always above zero. RMSE is an indicator of the fit between an estimate and real data points. Smaller RMSE reflects greater accuracy [112].

Chapter 4

Results and Discussion

The main objective of this thesis, as mentioned earlier, is to produce stable computer simulations of a system of point particles under the effect of LJ potential by using NVT-MC technique in order to get a mathematical formula as a function of reduced temperature (T^*) and reduced density ρ^* for the optimum maximum allowed displacement (O-d_{max}) that associated with the acceptance rate of 50% in three dimensional case (3D). An NVT-MC code was written in C^{++} language using C^{++} builder 6 and tested on Windows 2007, 32 bit. Once the simulation runs stable measurements of respective energy is performed. The output data files was saved in Microsoft Excel format, and the output figures was saved as output Matlab figures. The reason for installing C^{++} builder 6 instead of the other builders is that, it could be linked directly with Matlab 2008, and Microsoft office excels 2010. In NVT-MC code, the right balance between readability, taking advantage of C^{++} features, and performance have been considered in this thesis. The LJ potential energy behavior of the point particles, that simulated in 3D lattice, is studied to obtain the O-d_{max} that leads to get fast equilibration optimally with minimum number of MC sweeps. During the simulation, the calculations of the LJ potential follow the expected physical behavior,

and the periodic boundary conditions worked correctly.

The simulation using NVT-MC technique was chosen to simulate a system of 128 particles with 100000 MC sweeps. The number of particles and MC-sweeps are chosen to be sufficient to get the desired results. Also the values of the reduced temperature T^* and the reduced density ρ^* has been carefully chosen to cover both low and high conditions that the system could be in. In addition, the reduced cut off distance r^*_{cut} used in all simulations is 2.5. The choice of r^*_{cut} is very important as it affects the physical behavior of the system, and hence affects the accuracy of the mathematical calculations.

The choice of small r^*_{cut} values reduces the simulation time and cost. While the choice of large r^*_{cut} values leads to much simulation time and cost. The effect of the value of r^*_{cut} on the physical behavior of the LJ point particle system that simulated in this thesis, is studied and analyzed. Figures (1, 2, 3, and 4), show the LJ potential energy versus MC sweeps for simulation of 128 point particles at different T^* and ρ^* values for different values of r^*_{cut}. At low temperature (T^*=1) and for both low (ρ^*=0.25) and high (ρ^*=2) densities, the data presented in Figures (1, 2) shows that the LJ potential energy in the range r^*_{cut} (2.5-4) has almost the same values. Similarly, at high temperature (T^*=4.2) and for both low (ρ^*=0.25) and high (ρ^*=2) densities, the data presented in Figures (3, 4) shows that the LJ potential energy in the range r^*_{cut} (2.5-4) has almost the same values.

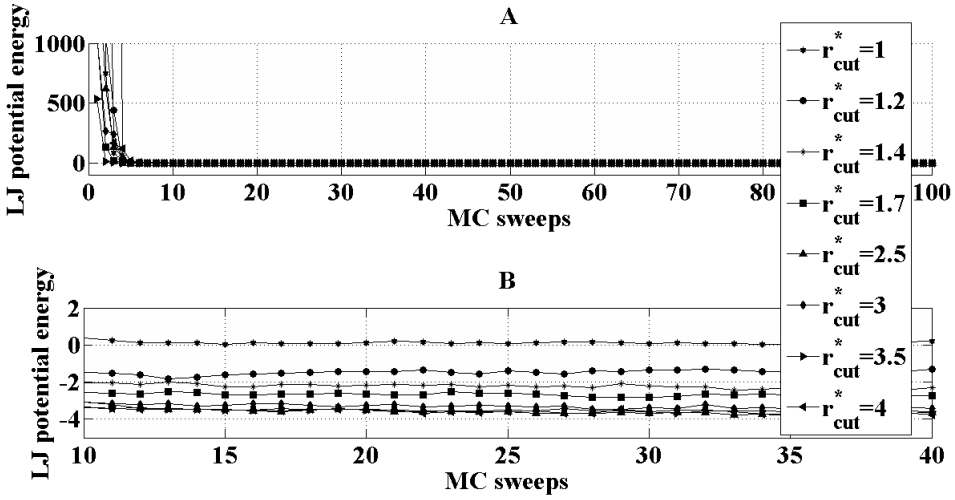

Figure 1: The simulation results which represents the relation between the LJ potential energy and MC sweeps for simulation of 128 particles using NVT-MC technique at T^*=1 and ρ^*=0.25 for different r^*_{cut} values. It is worth noting that sub-Figure (B) used to clarify the data presented in sub-Figure (A).

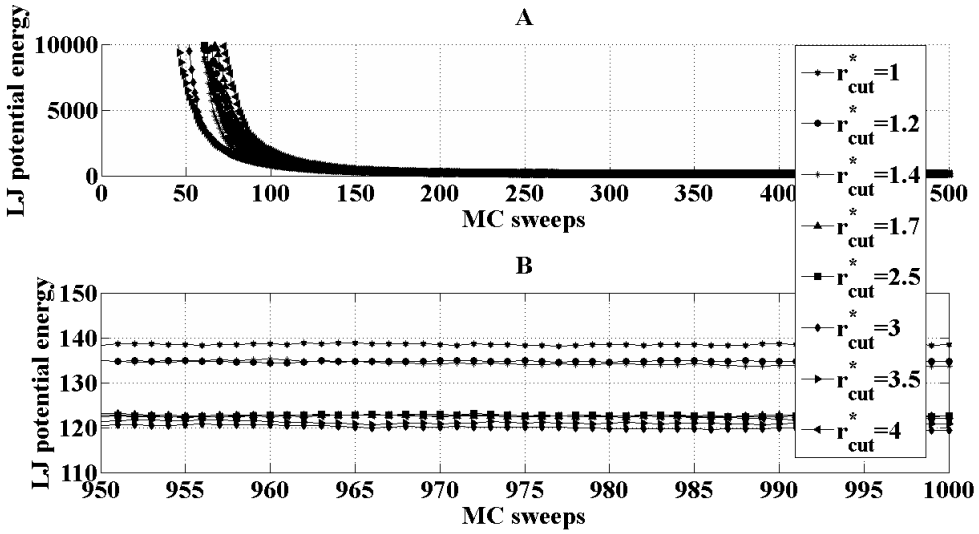

Figure 2: The simulation results which represents the relation between the LJ potential energy and MC sweeps for simulation of 128 particles using NVT-MC technique at T^*=1 and ρ^*=2 for different r^*_{cut} values. It is worth noting that sub-Figure (B) used to clarify the data presented in sub-Figure (A).

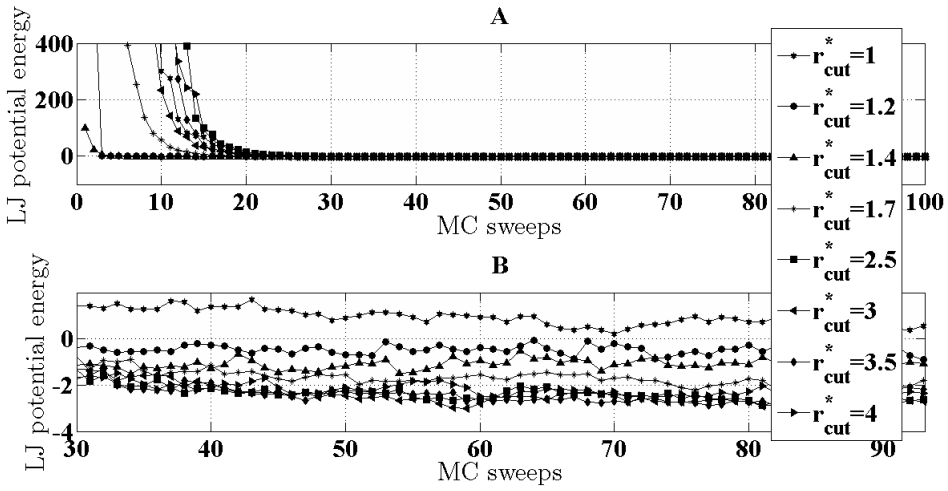

Figure 3: The simulation results which represents the relation between the LJ potential energy and MC sweeps for simulation of 128 particles using NVT-MC technique at T^*=4.2 and ρ^*=0.25 for different r^*_{cut} values. It is worth noting that sub-Figure (B) used to clarify the data presented in sub-Figure (A).

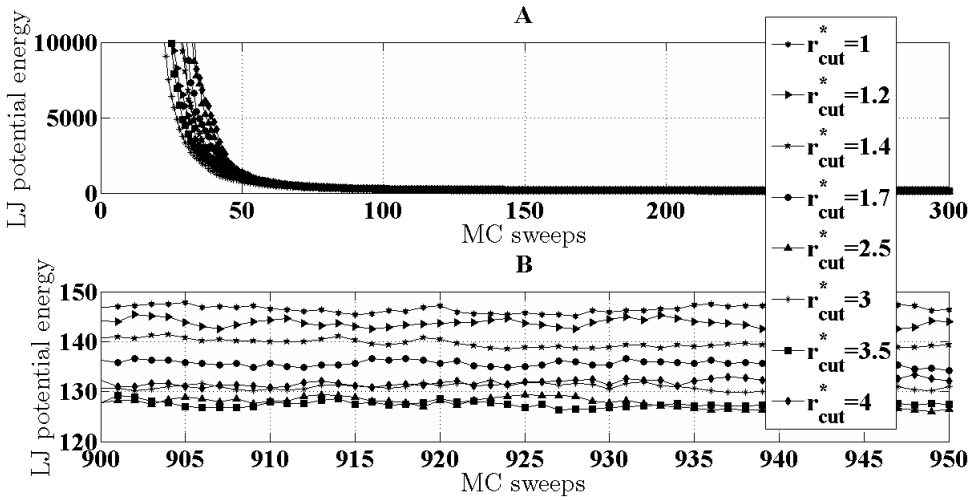

Figure 4: The simulation results which represents the relation between the LJ potential energy and MC sweeps for simulation of 128 particles using NVT-MC technique at T^*=4.2 and ρ^*=2 for different r^*_{cut} values. It is worth noting that sub-Figure (B) used to clarify the data presented in sub-Figure (A).

As mentioned earlier, the maximum allowed displacement (d_{max}) affects the value of the acceptance rate. For each value of T^* with fixed value of ρ^* or vice versa,

the O-d_{max} is chosen to be associated with the acceptance rate of 50%. Because there is no theoretical basis for the using the acceptance rate of 50% in MC simulation, different d_{max} values have been chosen to be associated with different acceptance rate values, and the behavior of the point particles under the effect of the LJ potential is simulated and studied using NVT-MC technique.

Figure (5) shows the LJ potential energy versus MC sweeps for the simulation of 128 point particles using NVT-MC technique at law temperature (T^*=1.5), and ρ^* =2 for different d_{max} values. The data presented in Figure (5) also shows the acceptance rate for each d_{max} value. It is clearly seen that the O-d_{max} have the best convergence to equilibrium. On the other hand, Figure (6) shows the LJ potential energy versus MC sweeps for the simulation of 128 particles using NVT-MC technique at high temperature (T^*=6), with ρ^* =2 for different d_{max} values. The data presented in the Figure (6) also shows the acceptance rate for each d_{max} value. Similarly, Figure (6) shows that the O-d_{max} have almost the best convergence to equilibrium.

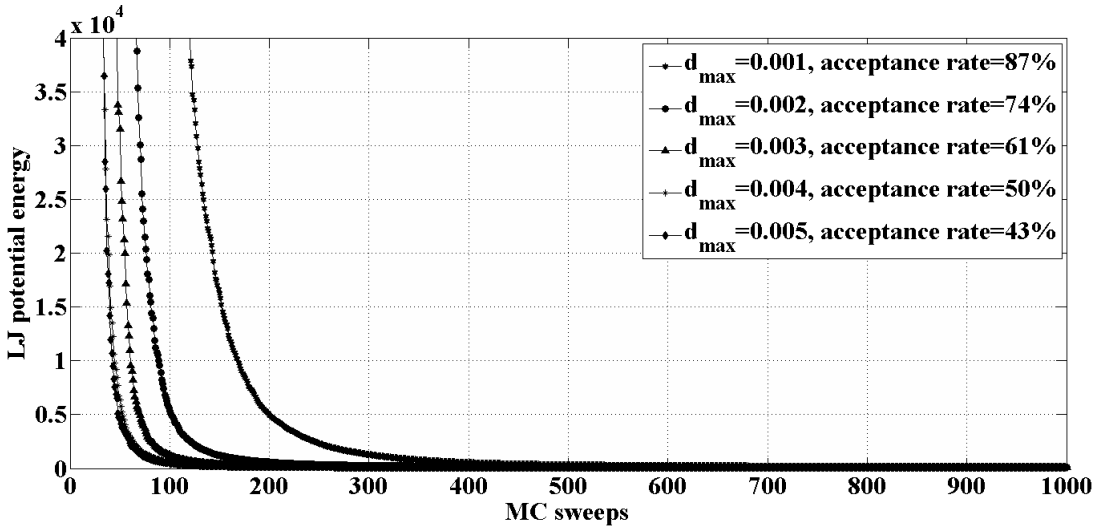

Figure 5: The simulation results which represents the relation between the LJ potential energy and MC sweeps for simulation of 128 particles using NVT-MC technique at T^*=1.5 and ρ^* =2 for different d_{max} values, with their associated acceptance rate values.

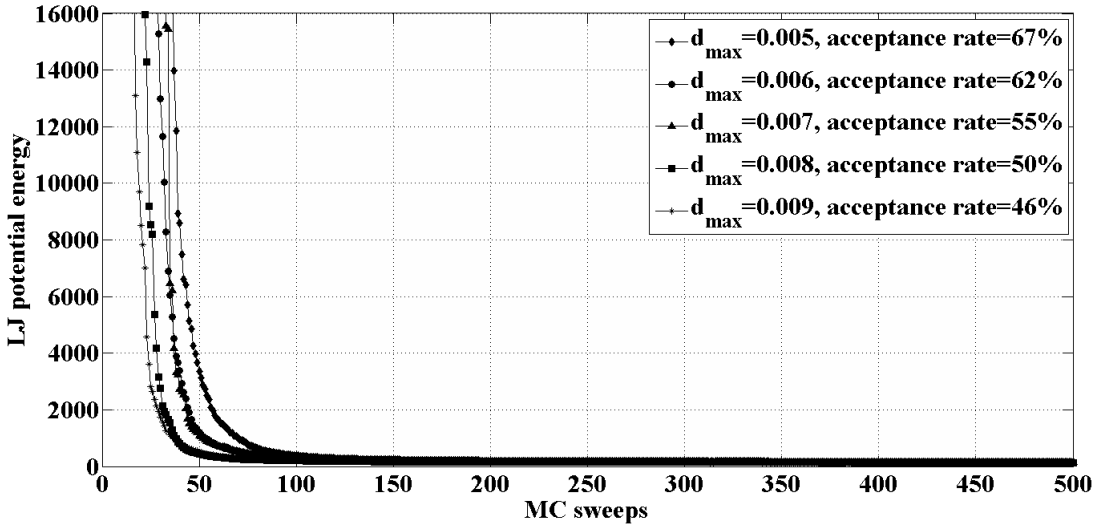

Figure 6: The simulation results which represents the relation between the LJ potential energy and MC sweeps for simulation of 128 particles using NVT-MC technique at T^*=6 and ρ^* =2 for different d_{max} values, with their associated acceptance rate values.

By considering the value of r^*_{cut}=2.5, a particular T^* was chosen and the simulation of 128-point particles system was started with different ρ^* values to find the O-d_{max} that associated with the acceptance rate of 50%. For example, at $T^* = 4.2$, the simulation was started at ρ^*=0.25 with some d_{max} values chosen by different trials. The results of this simulation as well as the best fitting curve are shown in Figure(7). The data presented in the Figure shows that the relation between the acceptance rate and d_{max} has an exponential form. By fitting the simulation results shown in Figure(7), using the fitting tool in Matlab, the best mathematical form with minimum error is given by

$$f = a\, e^{b\, d_{max}} + c\, e^{d\, d_{max}}, \tag{4.1}$$

where f is a function of d_{max} that represents the corresponding value of the acceptance rate. In Equation (4.1), a, b, c and d are constants which have the values

0.7779, -15.05, 0.3047, 0.1614, and 0.09329, respectively. The best statistical measures obtained from the fitting curve presented by Equation (4.1) are SSE=1.732e-005, R-square=0.9997, adjusted R-square=0.9995, and RMSE= 0.002403.

This procedure was repeated at T^*=4.2 for different values of ρ^* (ρ^*=0.3125, 0.375, 0.4375, 0.5, 0.625, 0.75, 1, 1.25, 1.5, 1.75, and 2) as shown in Figures (8, 9, 10, 11, 12, 13, 14, 15, 16, 17, 18), respectively. All the fitting curves shown in Figures (8-18) follow Equation (4.1) with different values for the constants a, b, c, and d as presented in Table (4.1). This implies that the constants a, b, c, and d depends on the value of ρ^*. The corresponding statistical measures regarding each curve for each ρ^* value are shown in Table (4.2). Since the values of the constants c and d are zero for almost all values of ρ^* (except at ρ^*=0.25), Equation (4.1) can be written as

$$f = a\, e^{b\, d_{max}}. \tag{4.2}$$

Equation (4.2) can also be written as

$$d_{max} = \frac{1}{b} \log\left(\frac{f}{a}\right). \tag{4.3}$$

Using Equation (4.3), the mathematical equation that can be used to get the O-d_{max} that associated with the acceptance rate of 50% is given by

$$O - d_{max} = \frac{\ln \frac{0.5}{a}}{b}. \tag{4.4}$$

Using Equation (4.4), and the values of the constants a, b that presented in Table (4.1), the values of O-d_{max} are calculated for each value of ρ^* at T^*=4.2 and the results are presented in Table (4.3).

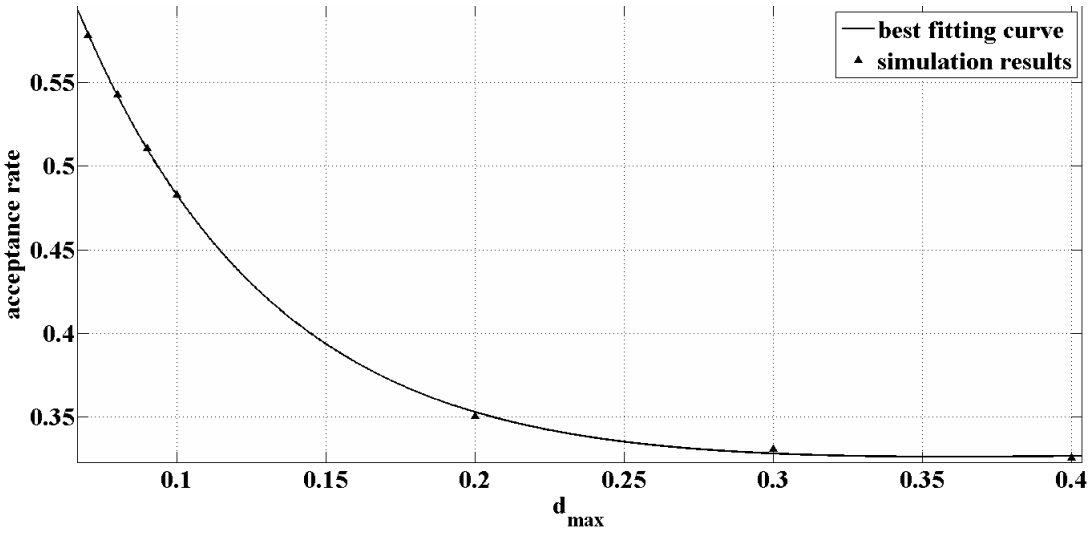

Figure 7: The simulation results and the best fitting curve which represents the relation between acceptance rate and d_{max} for simulation of 128 particles using NVT-MC technique for 100000 MC sweeps at T^*=4.2 and ρ^*=0.25. Statistical measures used is R-square = 0.9997.

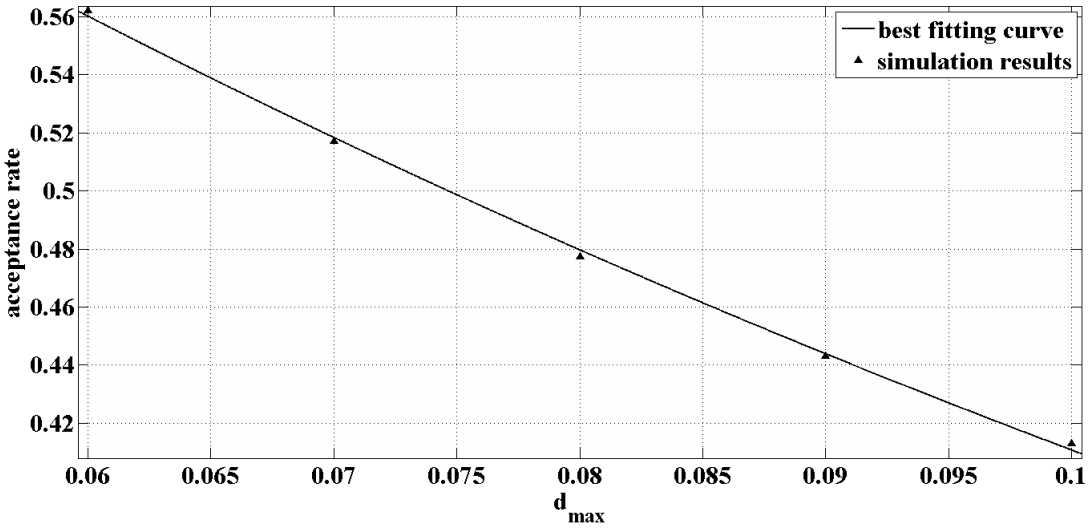

Figure 8: The simulation results and the best fitting curve which represents the relation between acceptance rate and d_{max} for simulation of 128 particles using NVT-MC technique for 100000 MC sweeps at T^*=4.2 and ρ^*=0.3125. Statistical measures used is R-square = 0.9988.

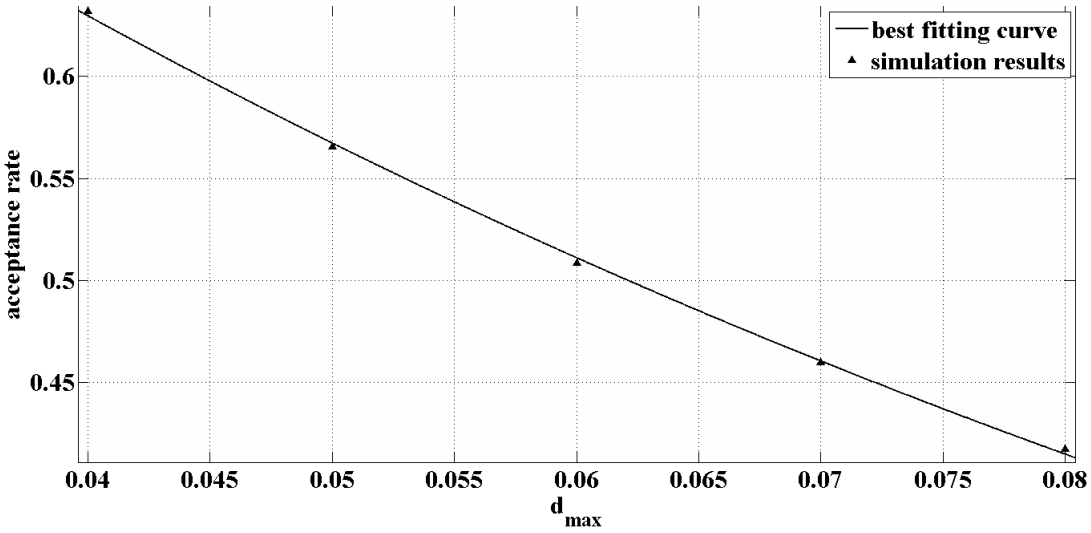

Figure 9: The simulation results and the best fitting curve which represents the relation between acceptance rate and d_{max} for simulation of 128 particles using NVT-MC technique for 100000 MC sweeps at T^*=4.2 and ρ^*=0.375. Statistical measures used is R-square = 0.9992.

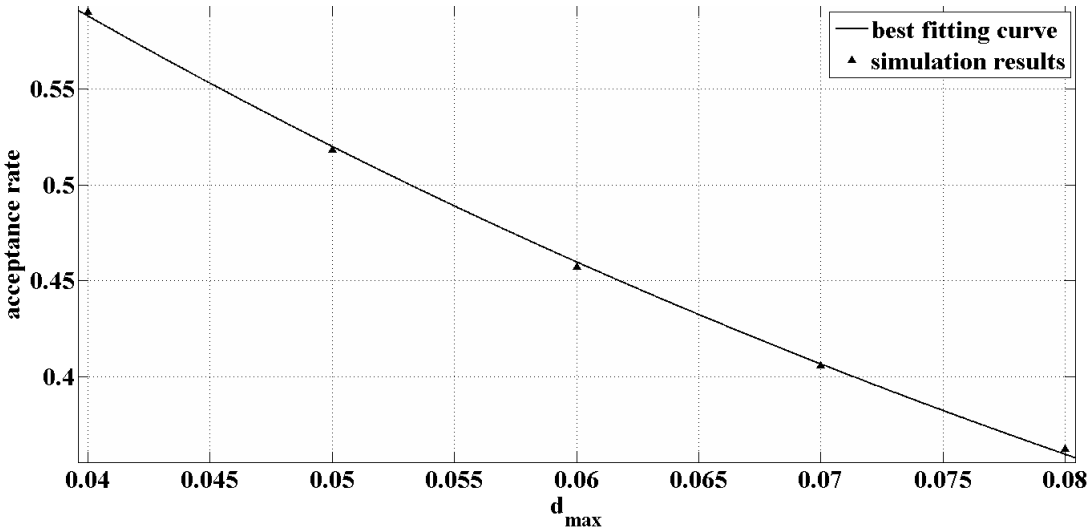

Figure 10: The simulation results and the best fitting curve which represents the relation between acceptance rate and d_{max} for simulation of 128 particles using NVT-MC technique for 100000 MC sweeps at T^*=4.2 and ρ^*=0.4375. Statistical measure used is R-square = 0.9993.

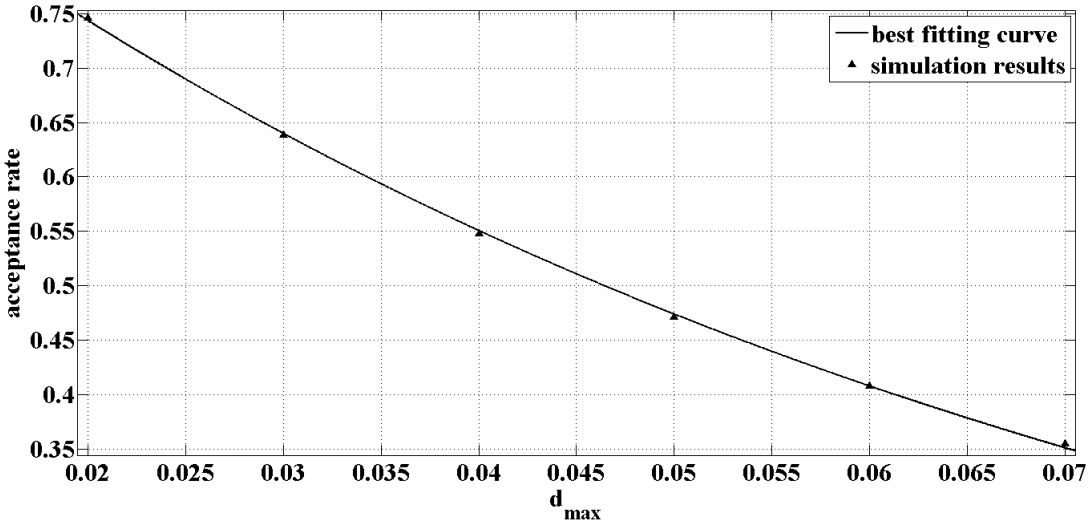

Figure 11: The simulation results and the best fitting curve which represents the relation between acceptance rate and d_{max} for simulation of 128 particles using NVT-MC technique for 100000 MC sweeps at T^*=4.2 and ρ^*=0.5. Statistical measure used is R-square = 0.9996.

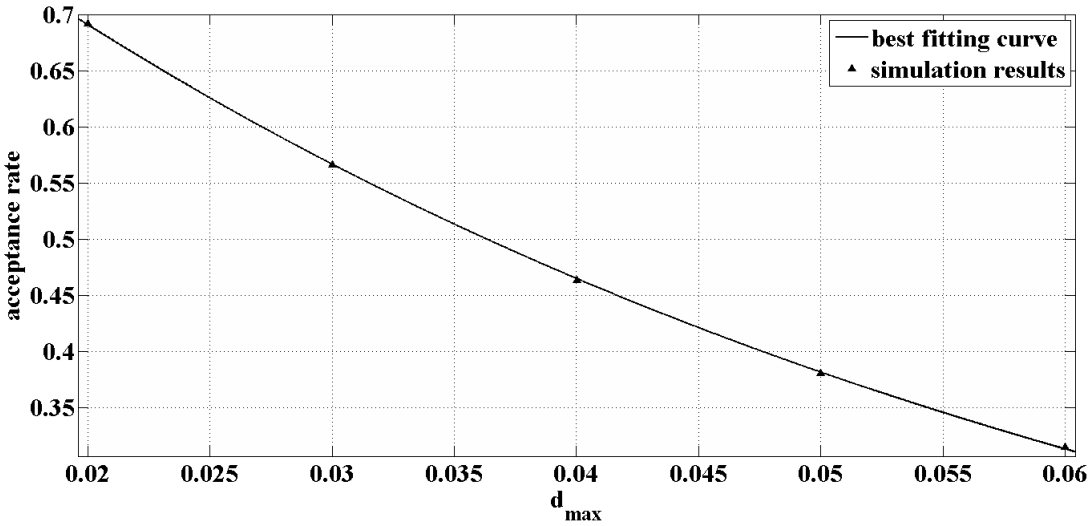

Figure 12: The simulation results and the best fitting curve which represents the relation between acceptance rate and d_{max} for simulation of 128 particles using NVT-MC technique for 100000 MC sweeps at T^*=4.2 and ρ^*=0.625. Statistical measure used is R-square = 0.9999.

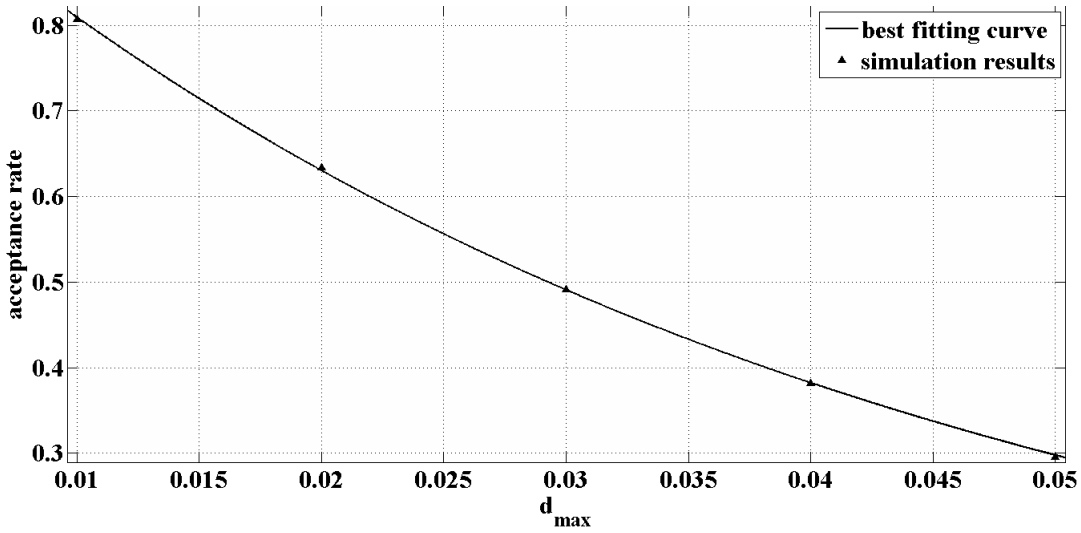

Figure 13: The simulation results and the best fitting curve which represents the relation between acceptance rate and d_{max} for simulation of 128 particles using NVT-MC technique with 100000 MC sweeps at T^*=4.2 and ρ^*=0.75. Statistical measure used is R-square = 0.9998.

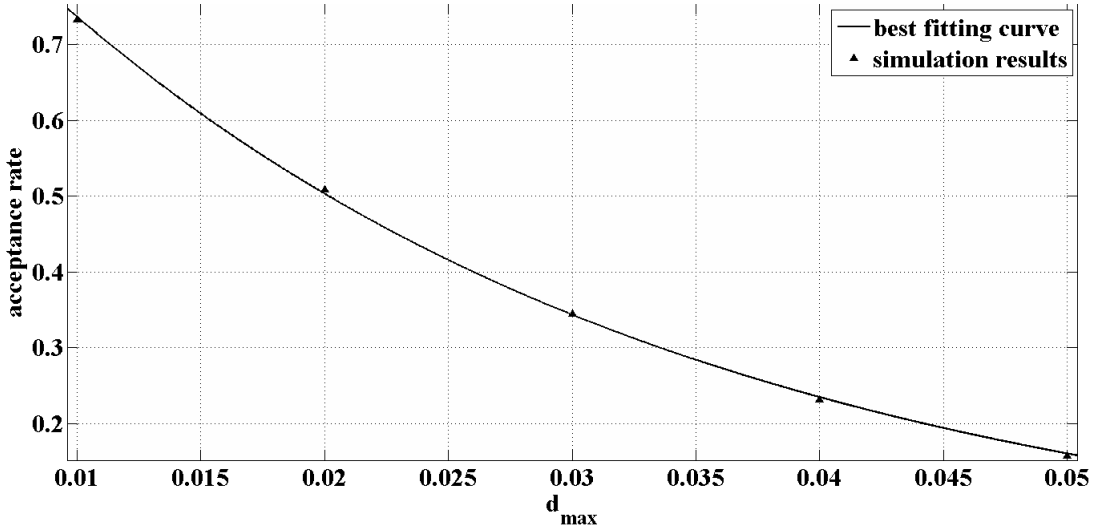

Figure 14: The simulation results and the best fitting curve which represents the relation between acceptance rate and d_{max} for simulation of 128 particles using NVT-MC technique for 100000 MC sweeps and T^*=4.2 and ρ^*=1. Statistical measure used is R-square = 0.9997.

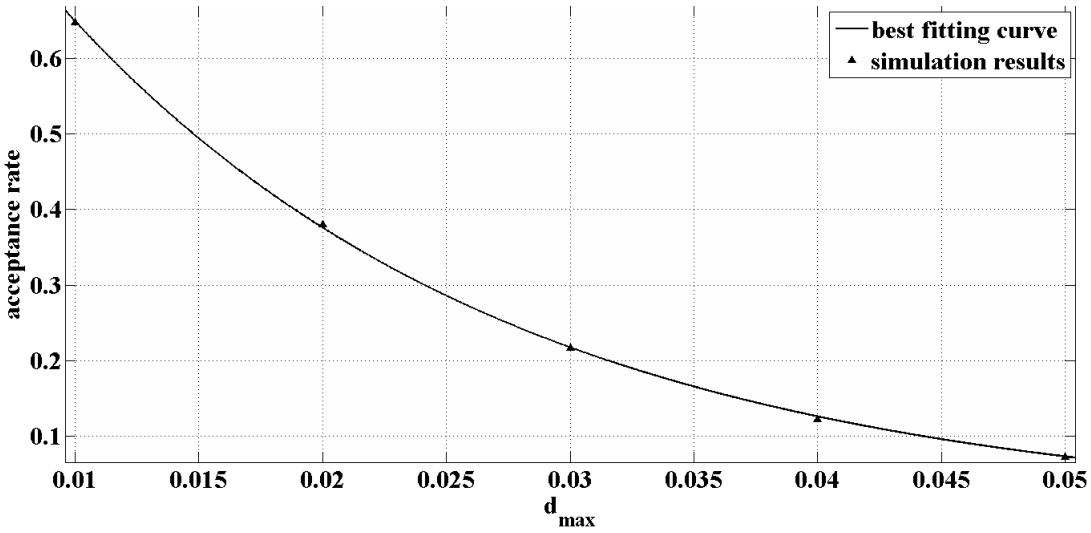

Figure 15: The simulation results and the best fitting curve which represents the relation between acceptance rate and d_{max} for simulation of 128 particles using NVT-MC technique for 100000 MC sweeps and T^*=4.2 and ρ^*=1.25. Statistical measure used is R-square = 0.9998.

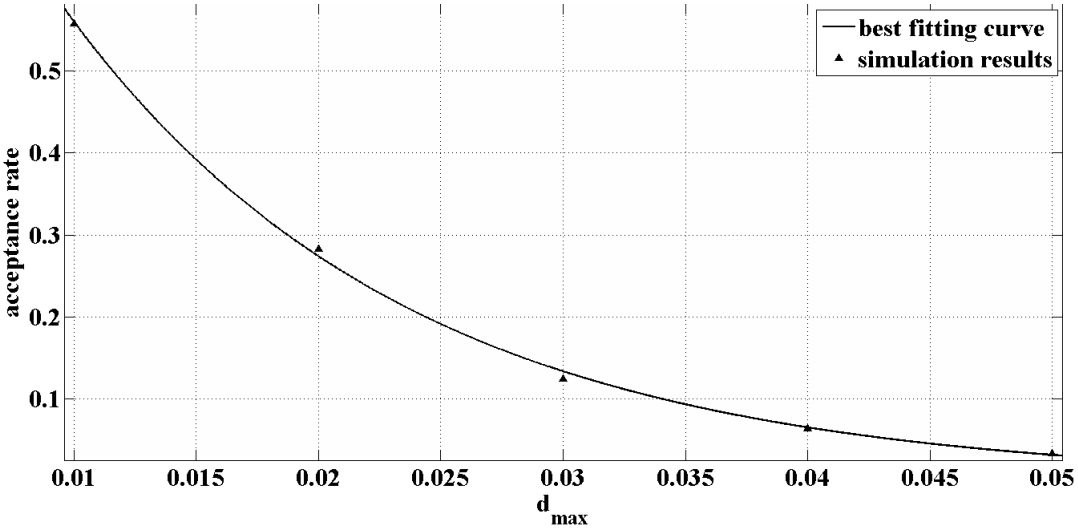

Figure 16: The simulation results and the best fitting curve which represents the relation between acceptance rate and d_{max} for simulation of 128 particles using NVT-MC technique for 100000 MC sweeps at T^*=4.2 and ρ^*=1.5. Statistical measure used is R-square = 0.9991.

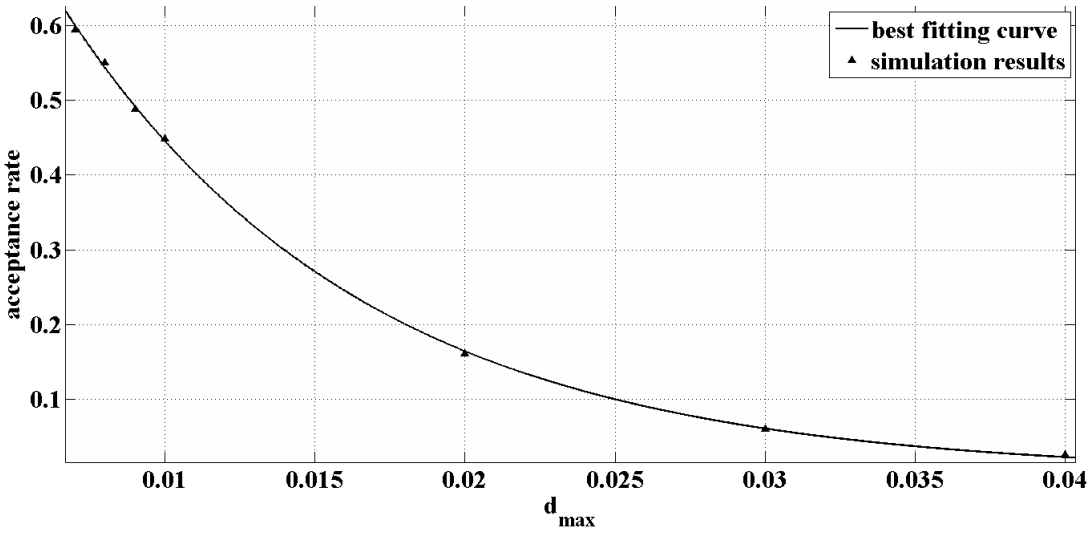

Figure 17: The simulation results and the best fitting curve which represents the relation between acceptance rate and d_{max} for simulation of 128 particles using NVT-MC technique for 100000 MC sweeps at T^*=4.2 and ρ^*=1.75. Statistical measure used is R-square = 0.9996.

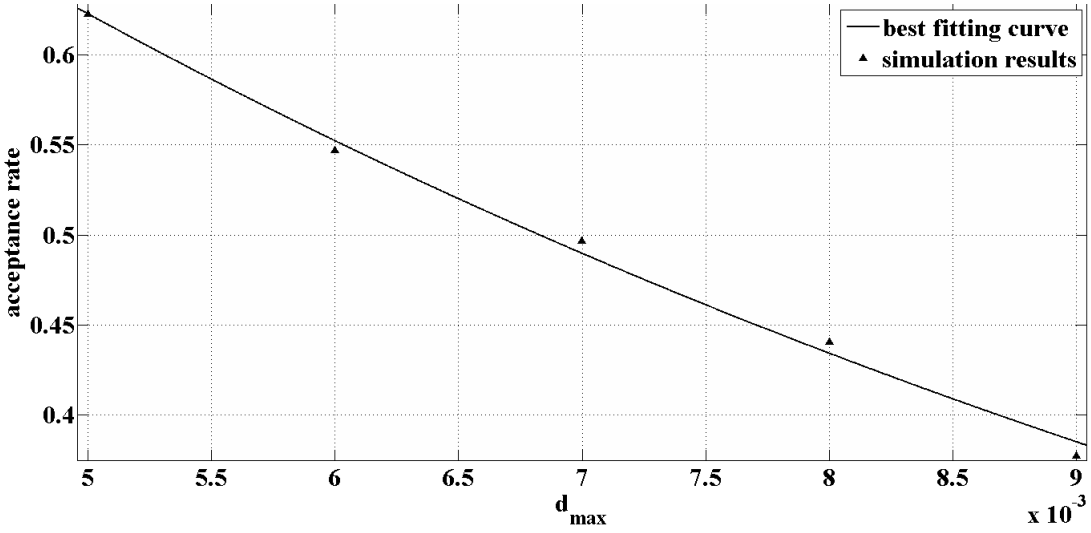

Figure 18: The simulation results and the best fitting curve which represents the relation between acceptance rate and d_{max} for simulation of 128 particles using NVT-MC technique for 100000 MC sweeps at T^*=4.2 and ρ^*=2. Statistical measure used is R-square = 0.9951.

Table 4.1: The values of the constants a, b, c and d obtained from fitting the simulation results, that presented in Figures (8-18).

ρ^*	a	b	c	d
0.25	0.7779	-15.05	0.3047	0.1614
0.3125	0.8919	-7.753	0	0
0.375	0.9557	-10.43	0	0
0.4375	0.9612	-12.29	0	0
0.5	1.004	-15	0	0
0.625	1.027	-19.81	0	0
0.75	1.039	-25	0	0
1	1.078	-38.12	0	0
1.25	1.122	-54.7	0	0
1.5	1.145	-71.51	0	0
1.75	1.207	-99.76	0	0
2	1.135	-120	0	0

Table 4.2: Statistical measures obtained from fitting the simulation results, that presented in Figures (8-18).

ρ^*	$R-square$
0.25	0.9997
0.3125	0.9988
0.375	0.9992
0.4375	0.9993
0.5	0.9996
0.625	0.9999
0.75	0.9998
1	0.9997
1.25	0.9998
1.5	0.9991
1.75	0.9996
2	0.9951

Table 4.3: The values of the O-d_{max} that obtained from Equation (4.4) and the data shown in Table (4.1) at T^*=4.2 for different values of ρ^*.

ρ^*	$O - d_{max}$
0.25	0.09329
0.3125	0.074647997
0.375	0.062112748
0.4375	0.053179366
0.5	0.046475947
0.625	0.036334635
0.75	0.029256236
1	0.020153585
1.25	0.014776234
1.5	0.011586517
1.75	0.008834053
2	0.006831499

The values of O-d_{max} with the corresponding ρ^* values that presented in Table (4.3), with its best fitting curve, are plotted as shown in Figure (19).

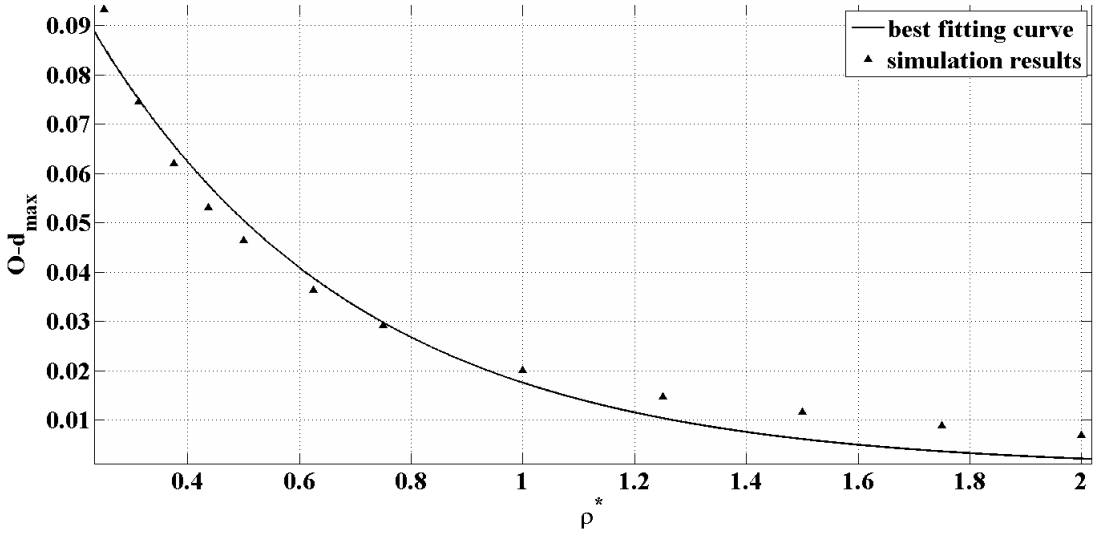

Figure 19: The simulation results and the best fitting curve which represents the relation between O-d_{max} and ρ^* for simulation of 128 particles using NVT-MC technique for 100000 MC sweeps at T^*=4.2 and different ρ^* values. Statistical measure used is R-square=0.9748.

The best curve represents the relation between O-d_{max} and ρ^* was found to be

$$g = k\, e^{l\,\rho^*}, \tag{4.5}$$

where g is a function of ρ^*, that represents O-d_{max} at $T^* = 4.2$. In Equation (4.5), k and l are constants which have the values 0.1451 and -2.114, respectively. The best statistical measure obtained from the fitting curve presented by Equation (4.5) is R-square=0.9748.

The above procedure was repeated for different values of T^* (T^*= 1, 1.5, 2, 2.5, 2.9, 3.4, 3.8, 4.2, 5 and 6). At each value of T^*, the simulation was done for different values of ρ^* (ρ^*=0.25, 0.3125, 0.375, 0.4375, 0.5, 0.625, 0.75, 1, 1.25, 1.5, 1.75, 2). The simulation results with their fitting data for each values of T^* mentioned above are presented in Appendix(A). The data presented in Appendix(A) as well as the data obtained by using Equations(4.5, and 4.4) are plotted as shown in Figure(20) using the same procedure presented earlier.

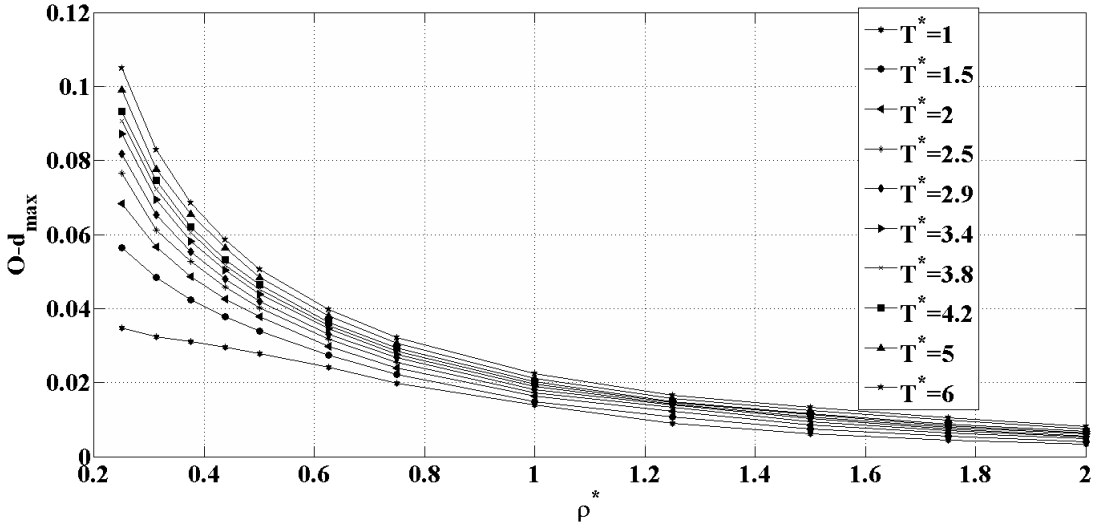

Figure 20: The values of the O-d_{max} versus ρ^* for simulation of 128 particles using NVT-MC technique for 100000 MC sweeps at different values of T^*.

It is worth noting that all the curves shown in Figure (20) satisfy the same mathematical formula that represented by Equation (4.5), with different values for the constants k and l. Table (4.4) shows the values of the constants k and l with the corresponding T^* value. This means that k and l depend on the value of T^* . Therefore, Equation (4.5) can be written as

$$g = k(T^*)e^{l\,(T^*)\rho^*}. \tag{4.6}$$

To obtain a mathematical formulas for k(ρ^*) and $l(\rho^*)$ as a functions of T^*, the relation between k and l versus T^*, with their best fitting curves, are plotted as shown in Figures (21) and (22), respectively. The best fitting curves for that shown Figures (21) and (22) are given by

$$k(T^*) = -0.2468T^{*-0.3376} + 0.2974. \tag{4.7}$$

$$l(T^*) = 0.9205T^{*-1.6} - 2.201. \tag{4.8}$$

Table 4.4: The values of the constants k and l obtained from fitting the simulation results, that presented if Figure (20).

T^*	k	l
1	0.05003	-1.279
1.5	0.08302	-1.728
2	0.1027	-1.896
2.5	0.1153	-1.975
2.9	0.1243	-2.024
3.4	0.1344	-2.083
3.8	0.1405	-2.104
4.2	0.1451	-2.114
5	0.1532	-2.12
6	0.1633	-2.149

Table 4.5: Statistical measures obtained from fitting the simulation results that presented if Figure (20)..

T^*	$R-square$
1	0.9913
1.5	0.9949
2	0.9874
2.5	0.9814
2.9	0.9784
3.4	0.9766
3.8	0.9752
4.2	0.9748
5	0.9719
6	0.9685

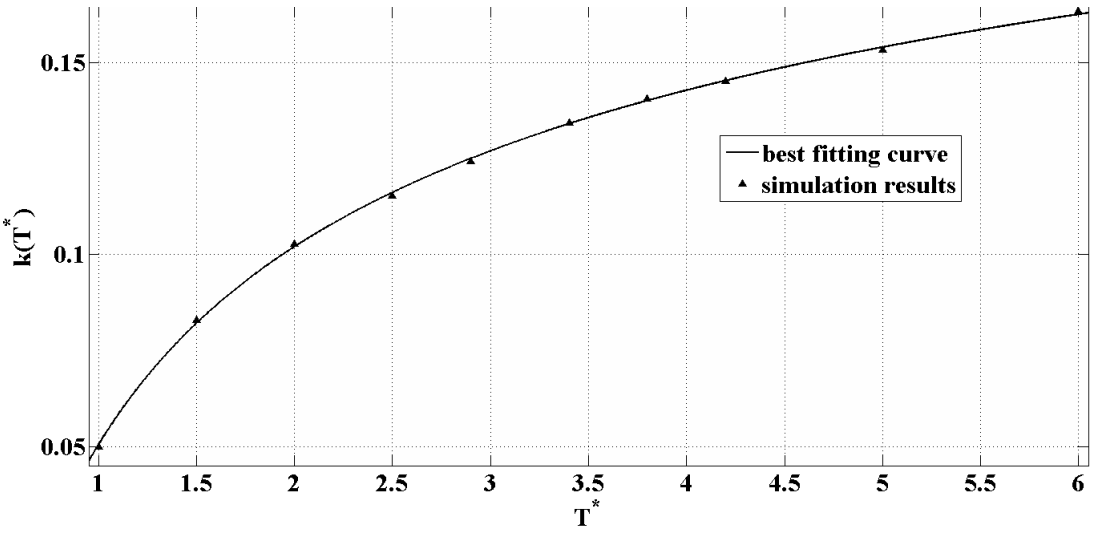

Figure 21: The constant k as a function of T^* as well as the best fitting curve obtained from the simulation of 128 particles using NVT-MC technique for 100000 MC sweeps. Statistical measure used is R-square = 0.9996.

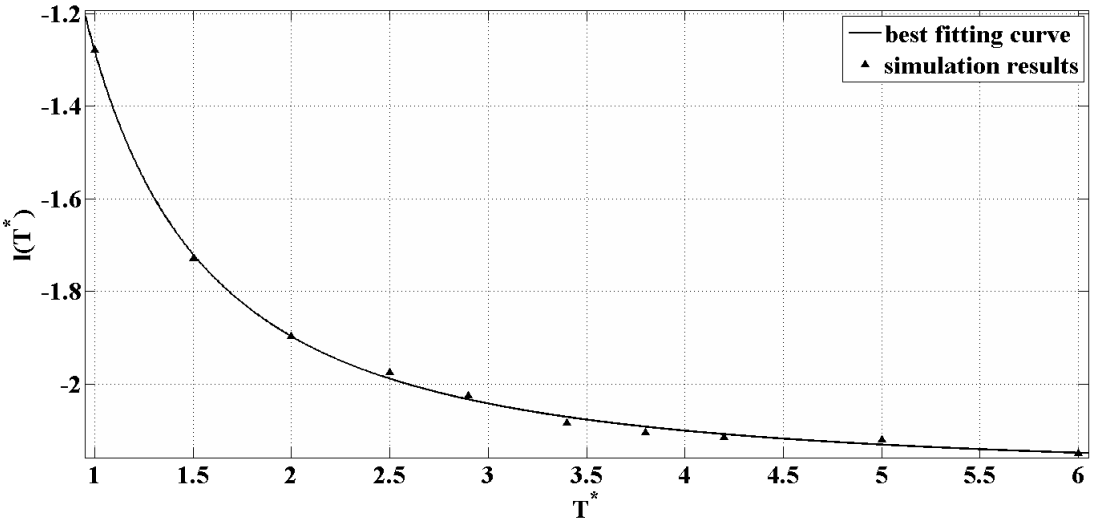

Figure 22: The constant l as a function of T^* as well as the best fitting curve obtained from the simulation of 128 particles using NVT-MC technique for 100000 MC sweeps. Statistical measure used is R-square = 0.9988.

To get a mathematical formula for O-d_{max} as a function of T^*, the simulation results shown in Appendix(A), again, are used to get that formula using the same procedure presented earlier. For example, Table(4.6) shows the values of O-d_{max} at different T^* values with ρ^*=1. The data presented in Table(4.6) are plotted as shown in Figure(23). Also, Figure(23) shows the best fitting curve for the simulation results. The data presented in the Figure clearly shows that the relation between O-d_{max} and T^* has an exponent form. By fitting the simulation results, using the fitting tool in Matlab, the best mathematical form with minimum error is given by

$$w = s\,T^{*\,h}, \tag{4.9}$$

where w is a function of T^* that represents O-d_{max} at $\rho^* = 1$. The values of the constants s and h have the values 0.01347 and 0.2796, respectively. The best statistical measure obtained from the fitting curve presented by Equation (4.9) is R-square=0.9953.

Table 4.6: The values of the O-d_{max}, as well as the best fitting curve, that obtained from the simulation of 128 particles using NVT-MC technique for 100000 MC sweeps at ρ^*=1 for different T^* values.

T^*	$O - d_{max}$
1	0.013899843
1.5	0.01481074
2	0.016246951
2.5	0.01728666
2.9	0.018060831
3.4	0.018933327
3.8	0.019569384
4.2	0.020153585
5	0.021211268
6	0.022353234

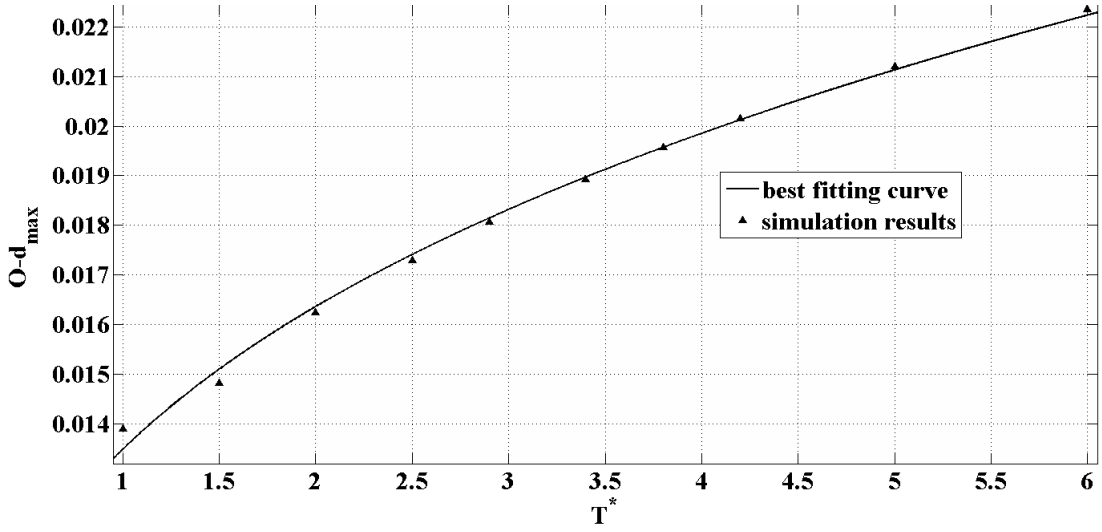

Figure 23: The values of the O-d_{max} versus T^* for simulation of 128 particles using NVT-MC technique for 100000 MC sweeps at ρ^*=1. Statistical measure used is R-square = 0.9953.

Again, the above procedure was repeated for different values of ρ^* (ρ^*= 0.25, 0.3125, 0.375, 0.4375, 0.5, 0.625, 0.75, 1, 1.25, 1.5, 1.75 and 2). For each value of ρ^*, the simulations were run for different values of T^* (T^*=1, 1.5, 2, 2.5, 2.9, 3.4, 3.8, 4.2, 5, and 6) and the results are plotted as shown in Figure (24). Therefore, Figure

(24) shows 12 curves, and each curve represents the relation between O-d_{max} and T^* at the corresponding ρ^* value.

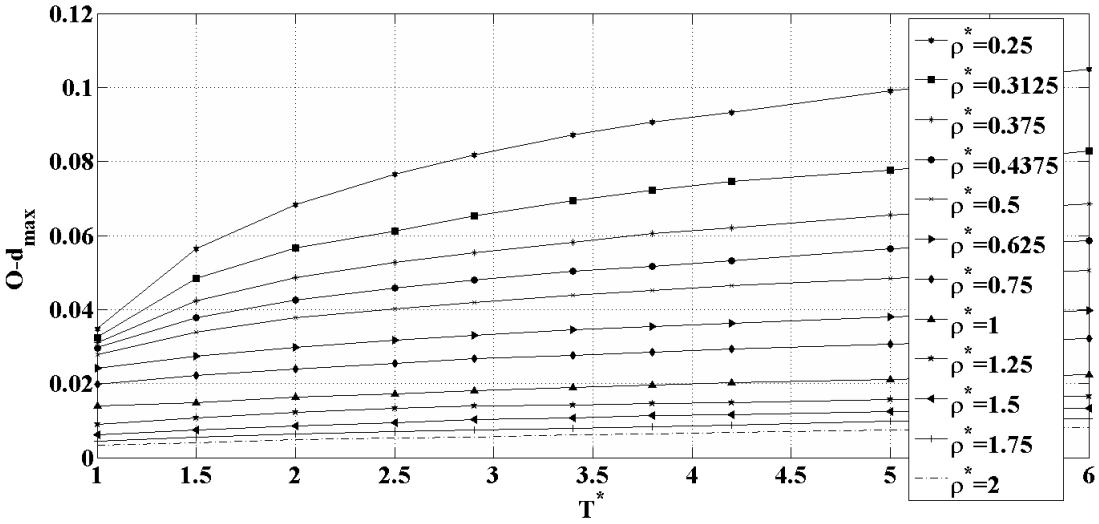

Figure 24: O-d_{max} versus T^*, as well as the best fitting curve, for simulation of 128 particles with 100000 MC sweeps for different ρ^* values

It is worth noting that all the curves shown in Figure (24) satisfy the same mathematical formula that represented by Equation (4.9), with different values for the constants s and h, that obtained form fitting the data presented in the Figure(24), using the fitting tool in Matlab. The values of the constants s and h are shown in Table (4.7). This means that s and h depend on the value of ρ^* . Therefore, Equation (4.9) can be written as

$$w = s(\rho^*)\, T^{*\, h(\rho^*)}, \tag{4.10}$$

To obtain a mathematical formulas for s(ρ^*) and h(ρ^*), the relation between s and h, versus ρ^* with their best fitting curves, are plotted as shown in Figures (4.11) and (4.12), respectively. The best fitting curves for the data shown in Figures (4.11) and (4.12) give

$$s(\rho^*) = 0.0668\rho^{*-1.599}. \tag{4.11}$$

$$h(\rho^*) = 0.9509e^{-4.382\rho^*} + 0.1489e^{0.6287\rho^*}. \tag{4.12}$$

Table 4.7: The values of the constants s and h obtained from the simulation of 128 particles using NVT-MC technique for 100000 MC sweeps for different values of ρ^*.

T^*	s	h
0.25	0.04639	0.4839
0.3125	0.03998	0.4282
0.375	0.03591	0.3806
0.4375	0.03262	0.3421
0.5	0.02978	0.3079
0.625	0.02455	0.2729
0.75	0.01982	0.2721
1	0.01347	0.2796
1.25	0.009645	0.3086
1.5	0.006446	0.4124
1.75	0.004478	0.4798
2	0.003337	0.4963

Table 4.8: Statistical measures obtained from the simulation of 128 particles using NVT-MC technique for 100000 MC sweeps at for different values of ρ^*.

T^*	$R-square$
0.25	0.9436
0.3125	0.9534
0.375	0.964
0.4375	0.9771
0.5	0.9846
0.625	0.9981
0.75	0.9996
1	0.9953
1.25	0.9732
1.5	0.9945
1.75	0.9981
2	0.9983

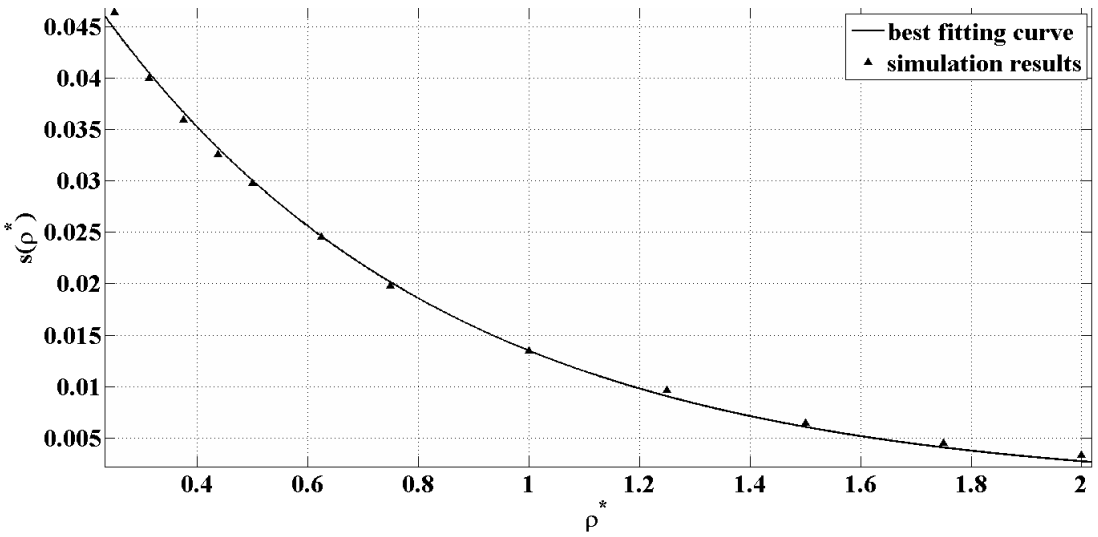

Figure 25: The constant s as a function of ρ^* as well as the best fitting curve obtained from the simulation of 128 particles using NVT-MC technique with 100000 MC sweeps. Its equation has the form represented by Equation (4.11). The statistical measure used is R-square = 0.9979.

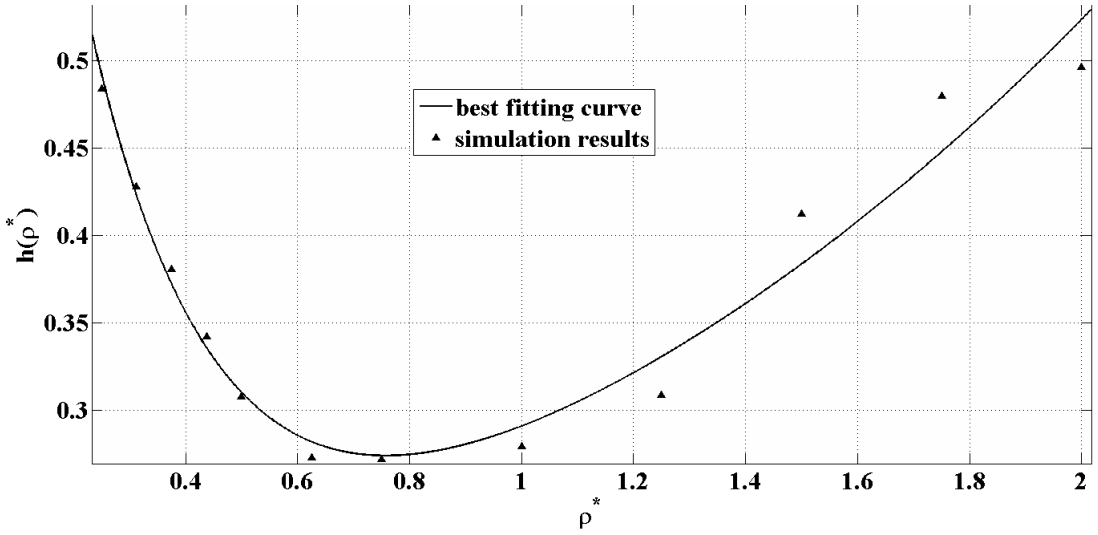

Figure 26: The constant h as a function of ρ^* as well as the best fitting curve obtained from the simulation of 128 particles using NVT-MC technique with 100000 MC sweeps. Its equation has the form represented by Equation (4.12). The statistical measures used is R-square = 0.9571.

To obtain the mathematical formula for O-d_{max} as a function of both T^* and ρ^*, the values of O-d_{max}, as well as the best fitting surface, are plotted using the

fitting tool in Matlab, as shown in Figure(27). The best mathematical expression that represents the relation between O-d_{max}, T^*, and ρ^* is given by

$$y(T^*,\rho^*) = 0.0526 + 0.034T^* - 0.1497\rho^* - 0.004354T^{*2} - 0.02704T^*\rho^* \\ +0.1311\rho^{*2} + 0.0002467T^{*3} + 0.001082T^{*2}\rho^* + 0.006881T^*\rho^{*2-0.03546}\rho^{*3}, \tag{4.13}$$

where y(T^*,ρ^*) represents the O-d_{max} at any T^* and ρ^* values.

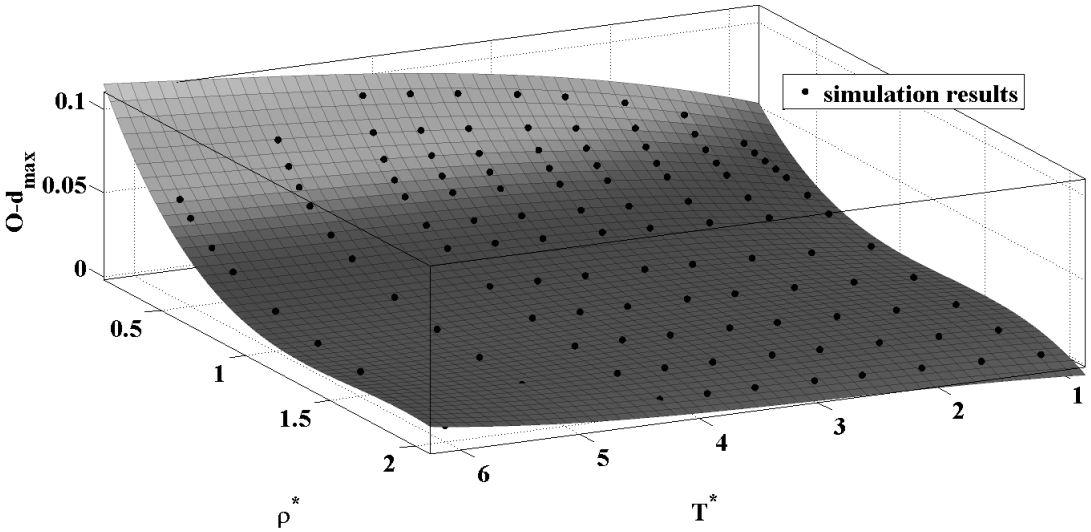

Figure 27: The best fitting surface obtained from the simulation of 128 particles using NVT-MC technique for 100000 MC sweeps at different T^* and ρ^* values. The mathematical Equation for the surface has the form represented by (4.13). The statistical measure used is R-square = 0.98.

4.1. Conclusions and Future work

A system of N-point particles with Lennard-Jones potential is simulated using Metropolis Monte Carlo method at constant number of particles, volume and temperature. The optimum cut off radius found for the Lennard-Jones potential is 2.5 in the dimensionless system. The periodicity of the system is considered in the calculations.

Number of particles used is N=128, which is sufficient in order to get good statistics results. Densities used are in the range [0.25,2], and the dimensionless temperature used is in the range [1,6]. The maximum allowed displacement d_{max} associated with 50% acceptance rate is found to be optimum. This gives the best convergence of simulation to the Lennard-Jones potential at equilibrium. Mathematical formula that represents the relation between d_{max} and acceptance rate is concluded and is represented by Equation (4.1) with accepted error values. At the acceptance rate 50% an explicit mathematical formula that describes the relation between temperature T^*, density ρ^* and the optimum maximum allowed displacement is concluded and is represented by Equation (4.13). As a future work, we are planning to add the kinetic energy calculations and take in our consideration the radius of the atom to apply the simulation at real systems. Moreover, we will incorporate the dipole-dipole interaction in the Lennard- Jones system, and find the optimum maximum allowed displacement of the angle and check out the relation between the best angle and best displacement obtained in this work.

Bibliography

[1] MAHENDRA JAIN. *Competition Science Vision, A specialized magazine for medical entrance and 10+2 exams*. Solved paper KCET, 98 and typical model papers.

[2] Born M. and Oppenheimer R. *Zur Quantentheorie der Molekeln, Annalen der Physik*. DOI: 10.1002/andp.19273892002 Volume 389, 457-484, 2006.

[3] Hirshfeld F. L. and Moreton Moore. *Crystallography Reviews, Electron Density Distributions in Molecules*. Department of structural chemistry, Weizmann Institute of Science, Rehovot, 76100, Israel, Volume 2, number 4, 1991.

[4] Nicholas J. Turro, V. Ramamurthy and J.C. Scaiano. *Principles of Molecular Photochemistry: An Introduction*. University Science Books, 2009.

[5] Kenneth R. Lang *Essential Astrophysics*. Springer, 128.

[6] Agrawal R. K., Garima Jain and Rekha Sharma. *Kinetic Theory and Thermodynamics*. Shashwat Agarwal, 1st edition, 1.56, 2006.

[7] Jeffery S. Marshall, Shuiqing Li. *Adhesive Particle Flow*. Cambridge University Press, 1st edition, 36, 2014.

[8] Hoare M.R. and Pal P. *Statics and stability of small cluster nuclei*. Nature Physical Science 230, 1971.

[9] Wales D.J and Dove J.P.K. *Global optimization by basin-hopping and the lowest energy structures of Lennard-Jones clusters containing up to 110 atoms.* J.Phys. Chem. A 101, 5111-5116, 1997.

[10] Cobera M., Llibre J. and Perez Chavela E..*Symmetric planar non-collinear relative equilipria for the Lennard-Jones potential 3-body problem with two equal masses.*

[11] Gustav Mie. *Zur Kinetischen Theorie der einatomigen Körper , Annalen der Physik.* DOI: 10.1002/andp.19033160802 Volume 316, 657-697, 2006.

[12] Salvatore Califano. *Pathways to Modern Chemical Physics.* Springer-Verlag Berlin Heidelberg, 2012.

[13] Edward Uhler Condon and G. H. Shortle. *The Theory of Atomic Spectra.* The press syndicate of the University of Cambridge the Pitt building, Trumpington street, Cambridge CB2 IRP, United Kingdom, Cambridge university press.

[14] Pietro Asinari, Eliodoro Chiavazzo and Prima edizione: Febbratio. *An Introduction to Multiscale Modeling with Applications*, 2013.

[15] Per Olov Lowdin. *Advances In Quantum Chemistry.* ACADEMIC PRESS, INC, Volume 22, 1991.

[16] Lennard-Jones J. E. Trans.Faraday Soc. 25, 668, 1929.

[17] Lennard-Jones J. E. (Cambridge) and Pike H. H. M. (Research Department, Woolwich). *The Determination of Inra-Molecular Forces From Measurements of Dipole Moments*, Read 13th April, 1934.

[18] Robert G. Mortimer. *Physical Chemistry.* British Library Cataloging in Publication Data, Elsevier Inc,420, 2008.

[19] William M. Spears and Diana F. Spears. *Physicomimetics: Physics-Based Swarm Intelligence*. Library of Congress Control Number: 2011942477 ACM Classifications : I.2, I.6, J.2, 443, 1998.

[20] Jayalatha K. Arockia; Rayappan and John Bosco Balaguru. *Lennard-Jones on Silver NanoparticlesAn Empirical Approach*. Journal of Computational and Theoretical Nesciences, Volume 11, Number 3, 568-572(5), 10.1166/jctn.2014.3396, 2014.

[21] David M. Heyes and Leslie V. Woodcock. *Fluid Phase Equilibria*. Volume 356, 301-308, DOI: 10.1016/j.fluid.2013.07.056, 2013.

[22] Sesma J. *Exact solution of the Schrödinger equation with a LennardJones (LJ) potential*. Journal of Mathematical Chemistry, Volume 51, Issue 7, 1881-1896, DOI: 10.1007/s10910-013-0189-9, 2013.

[23] Tai-Chia Lin and Bob Eisenberg.*A New Approach to the Lennard-Jones and a New Model: PNP-Steric Equations*. Communication in Mathematical Sciences, Volume 12, Issue 1, 149-173.

[24] Tatiana M. C. Faro, Gilmar P. Thim And Munir S. Skaf. *A Lennard-Jones plus Coulomb potential for AI3+ ions in aqueous solutions*. Journal of Chemical Physics, Volume: 132, Issue: 11, Article Number: 114509, DOI: 10.1063/103364110, 2010.

[25] Sergey A. Khrapak, Manis Chaudhuri and Gregor E. Morfill. *Liquid-solid phase transition in the Lennard-Jones system*. The American Physical Society, August 2010, Volume: 82, Issue: 5, Article Number: 052101, DOI: 10.1103/Phys, 2010.

[26] Pascal Richet. *The Physical Basis of Thermodynamics: With Applications to Chemistry*. Kluwer Academic / Plenum Publishers, new York 233 Spring Street, New York, New York 10013, 2001.

[27] Daan Frenkel and Berend Smit. *Understanding Molecular Simulation: From Algorithms to Applications*. Academic Press,1996-2002.

[28] Richard J. Sadus.*Molecular Simulation of Fluids Theory, Algorithms and Object-Orientation* . ELSEVIER, 1, 2002.

[29] Allen M. P. and Tildeseley D. J. *Computer Simulation of Liquids*. Oxford University Press, Walton Street, Oxford OX26DP.

[30] Robert Adolfovich Minlos. *Introduction to Mathematical Statistical Physics*. American Mathematical Society,47, 2000.

[31] Sanjay K. Nayak and Bhuvana k. P.. *ENGINEERING PHYSICS*. Tata McGraw Hill Education Private Limited, 2012.

[32] Jose Pujol. *Elastic Wave Propagation and Generation in Seismology*. Syndicate of the University of Cambridge, Jose Pujol, 2003.

[33] Dr. Agarwal P.K. and Dr. Sinha S.K. *Elements of Physics XI*. AGARWAL, 1st edition, ISBN: 978-81-7133-911-2, 2008-2009.

[34] Kaufui Vincent Wong. *Thermodynamics for Engineers*. CRC Press, Taylor and Francis Group, 1-15, 2012.

[35] Stephen J. Blundell and Katherine M. Blundell. *Concepts in Thermal Physics*. Oxford, 2nd edition, 38-39, 2010.

[36] Becky Lynn Eggimann. *Monte Carlo Simulations for NMR-based Protein Structure Determination*. ProQuest Information and Learning Company, 1,2, 2006.

[37] Armin Wachter and Henning Hoeber. *Compendium of Theoretical Physics*. Springer, 410-411, 2006.

[38] Guenault A.M. and Tony Guenault. *Statistical Physics*. Springer, ISBN: 978-1-4020-5975-9, 1988, 1995, 2007.

[39] Louis A. Girifalco. *Statistical Mechanics of Solids*. Oxford University Press, 2000.

[40] Kalyan Annamalai and Ishwar K. Puri. *Advanced Thermodynamics Engineering*, CRC Press LLC, 160, 2002.

[41] Nave C. R. *Force*. Hyperphysics. Dept. of Physics and Astronomy, Georgia State University. 2014.

[42] kip K.Sewell. *The Cosmic Sphere*. A Scientific Reformation, 1999.

[43] MAILOO SELVARATNAM. *A Guided Approach to Learning Chemistry*. Juta and Co, Ltd, 89, 1998-2006.

[44] Klaus D. Sattler. *Handbook of Nanophysics: Principles and Methods*. CRC press, 22-3, 2011.

[45] John Jewtt, Raymond Serway. *Physics for Scientists and Engineers with Modern Physics*. Cengage Learning, 198, 2013.

[46] Per Freiesleben Hansen and Ole Mejlhede Jensen. *The Science of Construction Materials*. Springer, 1.12-1.13, 2009.

[47] William Masterton, Cecile Hurley, and Edward Neth. *Chemistry: Principles and Reactions*. Cengage Learning, 7th edition, 209, 2011.

[48] *Concise Dictionary of Chemistry, A Perfect Reference for Aspirants of IAS, IIT-JEE, AIEEE, CBSE-PME, and Students of All Age Groups*. Editorial Board, V and PUBLISHERS, ISBN 978-93-815886-2-8, Edition: 2012.

[49] Daniel Reger, Scott Good, and David Ball. *Chemistry: Principles and Practice*. Cengage Learning, 3rd edition, 426, 2009.

[50] Ilya G. Kaplan. *Intermolecular Interactions: Physical Picture, Computational Methods and Model Potential*. John Wily and Sons Ltd. The Atrium, Southern Gate, Chichester, West Sussex PO19 8SQ, England, 2006.

[51] Darrell Ebbing and Steven D. Gammon. *General Chemistry*. Books/Cole, Cengage Learning, 3rd edition, 2013, 2011 .

[52] Oxtoby D. and Gillis H. and Campion, A. *Principles of Modern Chemistry*. Cengage Learning, ISBN: 9780534493660, 416, 2007.

[53] Moore J. and Stanitski C. and Jurs, P. *Principles of Chemistry: The Molecular Science*. Cengage Learning, ISBN: 9780495390794, 416, 2009.

[54] Jaiswal J. N. *Comprehensive Practical Physics XI*. LAXMI PUBLICATIONS(P) LTD.

[55] Rajan Dhaubhadel. *An Experimental Study of Dense Aerosol Aggregations*. KANSAS STATE UNIVERSITY, 2008.

[56] Walter Kauzmann. *Quantum Chemistry: An Introduction*. Elsevier, ISBN: 9781483270807, 503, (2013).

[57] Paul C. Hiemenz and Raj Rajagopalan. *Principles of Colloid and Surface Chemistry*. Marcel Deckker, Inc. 469, 3rd edition, 1997.

[58] OXTOPY, GILLIS and CAMPION. *Principles of Modern Chemistry*. Brooks/Cole Cengage Learning, 7th edition, 239, 2008-2012.

[59] Siegmund Brandt. *The Harvest of a century: Discoveries in Modern Physics in 100 Episodes*. Oxford university Press.

[60] Mingos D.M.P. and Wales D.J. *STRUCTURE AND BONDING, Intermolecular Forces and Clusters I*. Springer-Verlag, Berlin, Heidelberg, 2005.

[61] Tatjana Jeveremovic. *Nuclear Principles in Engineering*. Springer, ISBN: 978-0-387-85607-7, 2nd edition, 50, 2009.

[62] *Kaplan MCAT General Chemistry*. Kaplan Inc., 2009-2010.

[63] Normand M. Laurendeau. *Statistical Thermodynamics: Fundamentals and Applications*. Cambridge University Press, 2005.

[64] Mathendra Jain. *Competition Science Vision*. A Specialized Magazine for Medical Entrance.1999.

[65] Brian C. Smith. *Infrared Spectral Interpretation: A Systematic Approach*. CRC Press LLC, 9, 1999.

[66] Thomas F. George, Henk F. Arnoldus. *Theoretical Physics 2002*. Nova Science Publishers, Inc, Part 2, 210, 2002.

[67] Kawakatsu T. *Statistical Physics of Polymers*. Springer, 23, 2004.

[68] Sascha Sadewasser, Thilo Glatzel. *Kelvin Probe Force Microscopy: Measuring and Compensating Electrostatic Forces*. Springer, 10, 2012.

[69] Myron W. Evans. *Advances in Chemical Physics, Dynamical Processes in Condensed Matter*. John Wily and Sons, Inc, Volume LXIII, 295,1985.

[70] Srinivas Aluru. *Handbook of Computational Molecular Biology*. Taylor and Francis Group, LLC, 34-6, 2006.

[71] Mansel Davies, A. Hinchliffe. *Chemical Modeling: Application and Theory*. Henry Ling Ltd, Dorchester, Dorset, UK, Volume 4, 26, 2006.

[72] Tomás Diaz de la Rubia. *Scientific Modeling and Simulations*. Springer-Verlag, 31, 2009.

[73] Donglu Shi. *NanoScience in Biomedicine*. Tsinghua University Press, Beijing and Springers-Verlag GmbH Berlin Heidelberg, 49, 2009.

[74] Jacob N. Israelachvili. *Intermolecular and Surface Forces*. Elsevier Inc., 3rd edition, ISBN: 978-0-12-375182-9, 45, 2011.

[75] Geogios M. Kontogerogis and Georgios K. Folas. *Thermodynamic Models for Industrial Applications From Classical and Advanced Mixing Rules To Association Theories*. John Wiley and Sons Ltd, 20. 2010.

[76] Kurt Binder, P. David Landau. *A Guide to Monte Carlo Simulations in Statistical Physics*. Cambridge University Press, 3rd edition, 225, 2009.

[77] Satoh A. *Introduction to Molecular Microsimulation for Colloidal Dispersions*. Elsevier Science B. V. , 17th edition, 167, 2003.

[78] Joshua L. Hurst. *Transport Coefficient Computation Based on Input/output Reduced Order Molecules*. Doctorate Thesis, 17th edition, 133, 2008.

[79] Amiya K. Jana. *Chemical Process Modeling and Computer Simulation*. Prentice-Hall of India Private Limited, (2008).

[80] Eduardo MASSAD, Neli Regina Siqueira Ortega Laecio Carvalho de Barros and Claudio J. Struchiner. *Fuzzy Logic in Action: Applications in Epidemiology and Beyond*. Springer-Verlag Berlin Heidelberg, 2008.

[81] Lewis P. W. A. and Ed McKenzie. *Simulation Methodology for Statisticians Operations Analysts, and Engineers*. Wadsworth, Inc. Belmont, California 94002, Volume 1, 1989.

[82] Landua D. P. and Binder K. *A guide to Monte Carlo simulations in statistical physics*. Cambridge University Press, Cambridge, 2000.

[83] Newman M. E. J. and Barkema G. T. *Monte Carlo methods in Statistical Physics*. Clarendon Press, Oxford. ISBN: 0198517971, 9780198517979, 1999.

[84] Bendanov V. M. *Long-range order in a classical two-dimensional dipole system*. Journal of Physics: Condensed Matter, 4:75-82, 1992

[85] Navedeep Singh, Debjyoti Banerjee. *Nanofins Science and Applications*. Springer, ISBN: 978-1-4614-8531-5, 27, 2014.

[86] Philippe Ungerer, Bernard Tavitian, and Anne Boutin., *Applications of Molecular Simulation in the Oil and Gas Industry*. Editions Technip, ISBN: 2-7108-0858-7, 18, 2005.

[87] http://ocw.mit.edu/courses/materials-science-and-engineering/3-320-atomistic-computer-modeling-of-materials-sma-5107-spring-200).

[88] Preetisri Baskaran. *Computer Simulation of Protein Superabsorbents*. University of Boras, Master Thesis, 2011.

[89] Allen M.P. and Tildesly D.j. . *Computer simulation of liquids*. Oxford (UK): Oxford University Press, 1987.

[90] Metropolis, Nicholas. *The beginning of the Monte Carlo method*. Los Alamos Science 15.584 , 125-130, 1987.

[91] comte de Buffon, Georges Louis Leclerc. *Essai d'arithmétique morale*. 1777.

[92] David M. Ferguson, Ilja J. Siepmann, and Donald G. Truhlar., *Monte Carlo Methods in Chemical Physics*. John Wiley and Sons, Volume 105, ISBN: 0-471-19630-4, 245, 1999.

[93] Abdel-Rahman Mustafa Abu-Labda. *Monte Carlo simulations for classical two-dimensional dipolar antiferromagnetic systems on a square lattice*. St. John's Newfoundland and Labrador, Canada, 2004.

[94] Peter G. Flesch. *Light and Light Sources: High-Intensity Discharge Lamps*. Springer-Verlag Berlin Heidelberg, Netherlands, 51, 2006.

[95] Samuel G. Greenberg.*Random Sampling of Lattice Configurations Using Local Markov Chains*. ProQuest LLC, 9, 2009.

[96] Inessa G. Im. *Predicting Protein Secondary Structure Using Markov Chain Monte-Carlo Simulation*. ProQuest LLC, 17, 2009.

[97] Robert G. Gallager. *Stochastic Processes: Theory for Applications*. Cambridge University Press, 165, 2013.

[98] Metropolis N., Rosenbluth A. W., Rosenbluth M. N.,Teller A. H. , and Teller E. *Equation of state calculations by fast computing machines*. The Journal of Chemical Physics, Volume 21, Issue 6 :1087-1092, 1953.

[99] Binder K. and Heermann D. W.*Monte Carlo Simulation in Statistical Physics*. Springer-Verlag Berlin Heidelberg, DOI: 10.1007/978 -3-642-03163-2, 5th edition, 2010.

[100] David Chandler.*Introduction to Modern Statistical Mechanics*. Oxford University Press, ISBN: 0195042778, 9780195042771, 1987.

[101] Donald Allan McQuarrie. *Statistical Mechanics*. University Science Books, ISBN: 1891389157, 9781891389153, 2000.

[102] Rao M., Pangali C., and Berne B. J., *On the force bias Monte Carlo simulation of water: methodology, optimization and comparison with molecular dynamics*, Mol. Phys., 37, 1773-1789, 1979.

[103] Linse P., *The convergence of simulation of asymmetric electrolytes with charge asymmetry 60:1*, J. Chem. Phys. 110, 3493-3501, 1999.

[104] Mbamala E. C., and Pastore G., *Optimal Monte Carlo sampling for simulation of classical fluids*, Physica A, 313, 312-320, 2002.

[105] Montani R. A., *On the Monte Carlo simulation in the α-Agl system: the influence of the maximum displacement allowed to particles*, J. phys. Chem. Solids, 53, 1211-1214, 1992.

[106] Jaster A., *An improved Metropolis algorithm for hard core systems Physica A*, 264, 134-141, 1999.

[107] Binder K., *Application of Monte Carlo Methods to Statistical Physics*, Rep.prog.Phys. 60, 487559, 1997.

[108] David Anderson Dennis Sweeneyand Thomas Williams. *Essentials of Modern Business Statistics with Microsoft Excel*. 5th edition, 529.

[109] Karen A. Randolph and Laura L. Myers. *Basic Statistics in Multivariate Analysis* Oxford University, 118, 2013.

[110] William Hepburn. *Proving antitrust damages, Legal and Economic Issues.* American Bar Association, 2nd edition, 152, 2010.

[111] Michael Baron. *Probability and Statistics for Computer Scientists.* Taylor and Francis Group LLC, 359, 2007.

[112] Neil J. Salkind. *Encyclopedia of Research Design.* SAGE Publications, 1288, 2010.

Appendices

Table 9: The values of the constants a, b, c and d obtained from fitting the output data that results from the simulation of 128 particles using NVT-MC technique for 100000 MC sweeps at T^*=1 and different ρ^* values.

ρ^*	a	b	c	d
0.25	0.9857	-19.49	0	0
0.3125	0.9949	-21.21	0	0
0.375	1	-22.37	0	0
0.4375	1.008	-23.65	0	0
0.5	1.018	-25.2	0	0
0.625	1.035	-30.16	0	0
0.75	1.063	-38.23	0	0
1	1.13	-58.66	0	0
1.25	1.125	-90.17	0	0
1.5	1.158	-134.5	0	0
1.75	1.159	-187	0	0
2	1.088	-232	0	0

Table 10: Statistical measures obtained from fitting the output data that results from the simulation of 128 particles using NVT-MC technique for 100000 MC sweeps at T^*=1 and different ρ^* values.

ρ^*	$R-square$
0.25	0.9981
0.3125	0.9984
0.375	0.9991
0.4375	0.9994
0.5	0.9998
0.625	0.9999
0.75	0.9999
1	0.9987
1.25	0.9992
1.5	0.9933
1.75	0.9939
2	0.9957

Table 11: The values of the O-d_{max} obtained by using Equation (4.4) and the data presented in Table (4.1) at T^*=1 for different ρ^* values.

ρ^*	$O - d_{max}$
0.25	0.034825241
0.3125	0.032439139
0.375	0.030985569
0.4375	0.029645469
0.5	0.027881847
0.625	0.024122964
0.75	0.019729068
1	0.013899843
1.25	0.008993348
1.5	0.006244175
1.75	0.004495747
2	0.003326845

Table 12: The values of the constants a, b, c and d obtained from fitting the output data that results from the simulation of 128 particles using NVT-MC technique for 100000 MC sweeps at T^*=1.5 and different ρ^* values.

ρ^*	a	b	c	d
0.25	0.8571	-9.552	0	0
0.3125	0.9119	-12.44	0	0
0.375	0.9375	-14.86	0	0
0.4375	0.9869	-17.95	0	0
0.5	1.015	-20.85	0	0
0.625	1.032	-26.42	0	0
0.75	1.056	-33.81	0	0
1	1.115	-54.15	0	0
1.25	1.173	-79.33	0	0
1.5	1.104	-105.2	0	0
1.75	1.184	-157.1	0	0
2	1.074	-190.8	0	0

Table 13: Statistical measures obtained from fitting the output data that results from the simulation of 128 particles using NVT-MC technique for 100000 MC sweeps at T^*=1.5 and different ρ^* values.

ρ^*	$R-square$
0.25	0.995
0.3125	0.9965
0.375	0.9984
0.4375	0.9993
0.5	0.9999
0.625	1
0.75	0.9999
1	0.9998
1.25	0.9998
1.5	0.994
1.75	0.9959
2	0.9952

Table 14: The values of the O-d_{max} obtained by using Equation (4.4) and the data presented in Table (4.1) at T^*=1.5 for different ρ^* values.

ρ^*	$O-d_{max}$
0.25	0.056422372
0.3125	0.048305646
0.375	0.042359074
0.4375	0.037880814
0.5	0.033958551
0.625	0.027427928
0.75	0.022112847
1	0.01481074
1.25	0.010748919
1.5	0.007529345
1.75	0.005487242
2	0.004007008

Table 15: The values of the constants a, b, c and d obtained from fitting the output data that results from the simulation of 128 particles using NVT-MC technique for 100000 MC sweeps at T^*=2 and different ρ^* values.

ρ^*	a	b	c	d
0.25	0.85	-7.767	0	0
0.3125	0.9344	-11.04	0	0
0.375	0.9423	-13.01	0	0
0.4375	0.9511	-15.14	0	0
0.5	0.9963	-18.29	0	0
0.625	1.022	-23.93	0	0
0.75	1.05	-30.99	0	0
1	1.107	-48.92	0	0
1.25	1.17	69.32	0	0
1.5	1.184	-100.9	0	0
1.75	1.226	-141.9	0	0
2	1.221	-186.7	0	0

Table 16: Statistical measures obtained from fitting the output data that results from the simulation of 128 particles using NVT-MC technique for 100000 MC sweeps at T^*=2 and different ρ^* values.

ρ^*	$R-square$
0.25	0.9968
0.3125	0.9975
0.375	0.9981
0.4375	0.9984
0.5	0.9992
0.625	0.9996
0.75	0.9999
1	0.9998
1.25	0.9993
1.5	0.9996
1.75	0.9975
2	0.9947

Table 17: The values of the O-d_{max} obtained by using Equation (4.4) and the data presented in Table (4.1) at T^*=2 for different ρ^* values.

ρ^*	$O - d_{max}$
0.25	0.068318302
0.3125	0.056639177
0.375	0.048709884
0.4375	0.042471011
0.5	0.037694933
0.625	0.029874997
0.75	0.023941186
1	0.016246951
1.25	0.012264151
1.5	0.008543565
1.75	0.006320677
2	0.004782096

Table 18: The values of the constants a, b, c and d obtained from fitting the output data that results from the simulation of 128 particles using NVT-MC technique for 100000 MC sweeps at T^*=2.5 and different ρ^* values.

ρ^*	a	b	c	d
0.25	0.8514	-6.957	0	0
0.3125	0.8477	-8.627	0	0
0.375	0.9179	-11.52	0	0
0.4375	0.9722	-14.53	0	0
0.5	1.007	-17.42	0	0
0.625	1.029	-22.79	0	0
0.75	1.046	-29.04	0	0
1	1.096	-45.4	0	0
1.25	1.161	-63.39	0	0
1.5	1.192	-91.24	0	0
1.75	1.168	-120.5	0	0
2	1.107	-152.2	0	0

Table 19: Statistical measures obtained from fitting the output data that results from the simulation of 128 particles using NVT-MC technique for 100000 MC sweeps at T^*=2.5 and different ρ^* values.

ρ^*	$R-square$
0.25	0.9981
0.3125	0.9984
0.375	0.9984
0.4375	0.9993
0.5	0.9997
0.625	0.9999
0.75	0.9998
1	0.9998
1.25	0.9993
1.5	0.9993
1.75	0.9972
2	0.9975

Table 20: The values of the O-d_{max} obtained by using Equation (4.4) and the data presented in Table (4.1) at T^*=2.5 for different ρ^* values.

ρ^*	$O-d_{max}$
0.25	0.076509121
0.3125	0.061193775
0.375	0.05273267
0.4375	0.045764174
0.5	0.040190746
0.625	0.031668918
0.75	0.025417374
1	0.01728666
1.25	0.013289618
1.5	0.009521917
1.75	0.007040996
2	0.005222082

Table 21: The values of the constants a, b, c and d obtained from fitting the output data that results from the simulation of 128 particles using NVT-MC technique for 100000 MC sweeps at T^*=2.9 and different ρ^* values.

ρ^*	a	b	c	d
0.25	0.8686	-6.752	0	0
0.3125	0.8617	-8.334	0	0
0.375	0.9697	-11.96	0	0
0.4375	0.9762	-13.97	0	0
0.5	1.006	-16.7	0	0
0.625	1.029	-21.86	0	0
0.75	1.059	-28.16	0	0
1	1.09	-43.15	0	0
1.25	1.164	-60.73	0	0
1.5	1.22	-87.46	0	0
1.75	1.125	-108	0	0
2	1.109	-142	0	0

Table 22: Statistical measures obtained from fitting the output data that results from the simulation of 128 particles using NVT-MC technique for 100000 MC sweeps at T^*=2.9 and different ρ^* values.

ρ^*	$R-square$
0.25	0.998
0.3125	0.9986
0.375	0.9992
0.4375	0.9994
0.5	0.9998
0.625	0.9999
0.75	0.9999
1	0.9997
1.25	0.9989
1.5	0.9996
1.75	0.9985
2	0.995

Table 23: The values of the O-d_{max} obtained by using Equation (4.4) and the data presented in Table (4.1) at T^*=2.9 for different ρ^* values.

ρ^*	$O - d_{max}$
0.25	0.081794227
0.3125	0.065310665
0.375	0.05538283
0.4375	0.047892583
0.5	0.041864027
0.625	0.033016223
0.75	0.026650293
1	0.018060831
1.25	0.013914203
1.5	0.010198926
1.75	0.007508613
2	0.005609901

Table 24: The values of the constants a, b, c and d obtained from fitting the output data that results from the simulation of 128 particles using NVT-MC technique for 100000 MC sweeps at T^*=3.4 and different ρ^* values.

ρ^*	a	b	c	d
0.25	0.8812	-6.503	0	0
0.3125	0.8779	-8.099	0	0
0.375	0.8998	-10.11	0	0
0.4375	0.9717	-13.19	0	0
0.5	0.9806	-15.35	0	0
0.625	1.023	-20.76	0	0
0.75	1.042	-26.55	0	0
1	1.084	-40.87	0	0
1.25	1.129	-57.33	0	0
1.5	1.11	-74.92	0	0
1.75	1.111	-99.97	0	0
2	1.118	-129.6	0	0

Table 25: Statistical measures obtained from fitting the output data that results from the simulation of 128 particles using NVT-MC technique for 100000 MC sweeps at T^*=3.4 and different ρ^* values.

ρ^*	$R-square$
0.25	0.9983
0.3125	0.9988
0.375	0.9984
0.4375	0.999
0.5	0.9993
0.625	0.9998
0.75	0.9999
1	0.9998
1.25	0.9996
1.5	0.9987
1.75	0.9929
2	0.9978

Table 26: The values of the O-d_{max} obtained by using Equation (4.4) and the data presented in Table (4.1) at T^*=3.4 for different ρ^* values.

ρ^*	$O-d_{max}$
0.25	0.087140784
0.3125	0.069505444
0.375	0.058117153
0.4375	0.050374452
0.5	0.043879904
0.625	0.034483944
0.75	0.027656841
1	0.018933327
1.25	0.014206863
1.5	0.010644784
1.75	0.007986473
2	0.006237896

Table 27: The values of the constants a, b, c and d obtained from fitting the output data that results from the simulation of 128 particles using NVT-MC technique for 100000 MC sweeps at T^*=3.8 and different ρ^* values.

ρ^*	a	b	c	d
0.25	0.8876	-6.332	0	0
0.3125	0.8867	-7.929	0	0
0.375	0.9404	-10.43	0	0
0.4375	0.945	-12.3	0	0
0.5	0.9891	-14.92	0	0
0.625	1.003	-19.71	0	0
0.75	1.052	-26.03	0	0
1	1.081	-39.4	0	0
1.25	1.11	-54.64	0	0
1.5	1.201	-76.4	0	0
1.75	1.128	-97.51	0	0
2	1.093	-122.2	0	0

Table 28: Statistical measures obtained from fitting the output data that results from the simulation of 128 particles using NVT-MC technique for 100000 MC sweeps at T^*=3.8 and different ρ^* values.

ρ^*	$R-square$
0.25	0.9985
0.3125	0.9988
0.375	0.9987
0.4375	0.9989
0.5	0.9994
0.625	0.9995
0.75	0.9999
1	0.9998
1.25	0.9978
1.5	0.9999
1.75	0.9974
2	0.9955

Table 29: The values of the O-d_{max} obtained by using Equation (4.4) and the data presented in Table (4.1) at T^*=3.8 for different ρ^* values.

ρ^*	$O - d_{max}$
0.25	0.090636938
0.3125	0.072253576
0.375	0.060565409
0.4375	0.051754214
0.5	0.045233336
0.625	0.035319264
0.75	0.028576269
1	0.019569384
1.25	0.014595666
1.5	0.011469918
1.75	0.008343691
2	0.006399946

Table 30: The values of the constants a, b, c and d obtained from fitting the output data that results from the simulation of 128 particles using NVT-MC technique for 100000 MC sweeps at T^*=5 and different ρ^* values.

ρ^*	a	b	c	d
0.25	0.771	-14.71	0.3148	0.1899
0.3125	0.829	-14.03	0.2167	0.3376
0.375	0.9502	-9.814	0	0
0.4375	0.9803	-11.92	0	0
0.5	1.004	-14.38	0	0
0.625	1.021	-18.77	0	0
0.75	1.036	-23.8	0	0
1	1.073	-36	0	0
1.25	1.114	-51.28	0	0
1.5	1.155	-66.88	0	0
1.75	1.056	-76.41	0	0
2	1.072	-102.6	0	0

Table 31: Statistical measures obtained from fitting the output data that results from the simulation of 128 particles using NVT-MC technique for 100000 MC sweeps at T^*=5 and different ρ^* values.

ρ^*	$R-square$
0.25	0.9997
0.3125	0.9998
0.375	0.999
0.4375	0.9984
0.5	0.9997
0.625	0.9998
0.75	0.9999
1	0.9998
1.25	0.9998
1.5	0.999
1.75	0.9981
2	0.9974

Table 32: The values of the O-d_{max} obtained by using Equation (4.4) and the data presented in Table (4.1) at T^*=5 for different ρ^* values.

ρ^*	$O-d_{max}$
0.25	0.09901
0.3125	0.07775
0.375	0.065423313
0.4375	0.056480751
0.5	0.048479778
0.625	0.03803568
0.75	0.030609846
1	0.021211268
1.25	0.015622159
1.5	0.012518653
1.75	0.009784523
2	0.007433462

Table 33: The values of the constants a, b, c and d obtained from fitting the output data that results from the simulation of 128 particles using NVT-MC technique for 100000 MC sweeps at T^*=6 and different ρ^* values.

ρ^*	SSE	$R-square$	$adjustedR-square$	$RMSE$
0.25	0.7849	-13.43	0.289	0.6109
0.3125	0.895	-7.035	0	0
0.375	0.956	-9.443	0	0
0.4375	0.9601	-11.15	0	0
0.5	0.965	-12.98	0	0
0.625	1.007	-17.6	0	0
0.75	1.041	-22.75	0	0
1	1.067	-33.91	0	0
1.25	1.106	-48.01	0	0
1.5	1.118	-60.63	0	0
1.75	1.07	-71.97	0	0
2	1.089	-96.05	0	0

Table 34: Statistical measures obtained from fitting the output data that results from the simulation of 128 particles using NVT-MC technique for 100000 MC sweeps at T^*=6 and different ρ^* values.

ρ^*	$R-square$
0.25	0.9999
0.3125	0.9995
0.375	0.9989
0.4375	0.9992
0.5	0.9993
0.625	0.9995
0.75	0.9999
1	0.9997
1.25	0.9998
1.5	0.9992
1.75	0.995
2	0.9991

Table 35: The values of the O-d_{max} obtained by using Equation (4.4) and the data presented in Table (4.1) at T^*=6 for different ρ^* values.

ρ^*	$O - d_{max}$
0.25	0.105
0.3125	0.082759861
0.375	0.068638125
0.4375	0.058513843
0.5	0.050656395
0.625	0.039779704
0.75	0.03223424
1	0.022353234
1.25	0.016536078
1.5	0.013272119
1.75	0.010571152
2	0.008104186